**National University of Science and Technology POLITEHNICA Bucharest**
**Doctoral School of Electrical Engineering**

# EXTENDED ABSTRACT
# Ph. D. THESIS

---

# Contributions to the Development of Electromagnetic Actuators

---

**Ph. D. Student,**
**Ing. Dragoș-Ștefan NICOLESCU**

**Ph. D. Supervisor,**
**Prof. Univ. Dr. Ing. Florea Ioan HĂNȚILĂ**

**BUCHAREST**
**2025**

# Content

# 1. Introduction

Electromagnetic actuators represent a distinct domain within electrical engineering, being one of the fields in which electromagnetic field theory has found immediate and practically useful applications.

Essentially, the concept of an actuator refers to a device that converts electromagnetic energy into kinetic energy [1][2]. These can be rotary —such as DC or AC current motors —or linear, with the most common being DC or AC current electromagnets, as well as electromagnetic suspensions and propulsion systems.

The model of a linear electromagnetic actuator with permanent magnets proposed in this thesis is similar in terms of operating principle and main parts to other existing designs. However, unlike the other models, this model features optimized positioning, dimensions, and magnetic field distrubution through the various components in order to achieve superior kinetic performance.

## Presentation of the Doctoral Research Topic

The novelty of this work lies in the development of a new geometric structure of the ferromagnetic circuit, so the electromagnetic actuator develops maximum force at the minimum air gap in the resting position, as well as during the closing maneuver, for a given volume. Thus, during design stage, the actuator's main dimensions considered technological and material limitations, resulting in an optimized structure. Numerical modeling of the actuator in its four functional states (i.e., resting at maximum and minimum air gap, as well as during closing and opening maneuvers) validated both the design and the operating principle of the actuator.

## Scope of the doctoral thesis

This doctoral thesis addresses scientific issues related to linear electromagnetic actuators with permanent magnets. The general objective of the thesis was to develop a high-performance linear electromagnetic actuator with permanent magnets and a novel geometric structure, aiming to enhance both electromagnetic and mechanical parameters.

This goal was pursued through the analysis of the main structural solutions adopted up to date, whose advantages and disadvantages are presented in the current state-of-the-art chapter of the thesis.

Secondary objectives were accomplished to validate the main goal, including: the mechanical analysis of the electromagnetic actuator to determine its main mechanical parameters; implementation of an experimental model to validate both the analytical and numerically obtained solutions; development of a power source for the linear electromagnetic actuator with permanent magnets to enable operation in various environments; experimental research to validate the actuator's electromagnetic and mechanical performance as predicted by numerical simulations.

The research results have been disseminated through scientific articles published in prestigious national and international journals. The main outcome of this thesis is represented by both the numerical and experimental models of the linear electromagnetic actuator with permanent magnets. An additional significant result is the experimental model of the actuator's power supply, which enables its use in various locations.

The doctoral thesis opens new perspectives for research and development of linear electromagnetic actuators with permanent magnets, particularly in the geometric design of their ferromagnetic circuits.

**Content of the doctoral thesis**

Chapter 2 presents the current state of the art in the field, detailing various geometric solutions for electromagnetic actuators with permanent magnets, while analyzing their advantages and limitations.

Chapter 3 introduces the development of a new model of electromagnetic actuator with permanent magnets. It discusses the operating principle of the actuator from both electromagnetic and kinetic point of views, emphasizing the electromechanical correlation of the device.

Chapter 4 addresses the analytical dimensioning of the main parts of the electromagnetic actuator, including the computation of the geometric dimensions of the ferromagnetic circuit and the key parameters of the excitation coil.

Chapter 5 presents a detailed numerical analysis of the current-fed electromagnetic actuator. A 2D finite element model was implemented using FEMM software to evaluate the actuator's behavior under various conditions.

Chapter 6 covers the kinematic analysis of the electromagnetic actuator, computing the developed force, acceleration, kinetic energy, and resulting velocity of the mobile armature to assess the device’s dynamic performance.

Chapter 7 details the implementation of the experimental model of the electromagnetic actuator, including technical drawings and figures of its main parts.

Chapter 8 focuses on the design, numerical modeling, and implementation of the power supply for the electromagnetic actuator.

Chapter 9 presents the experimental research conducted on the actuator, evaluating electromagnetic and mechanical parameters to verify its performance in actual operation.

Finally, Chapter 10 is dedicated to observations and conclusions regarding the entire development process of the electromagnetic actuator with permanent magnets and its associated power supply.

# 2. State of the Art in Electromagnetic Actuators with Permanent Magnets

## 2.1. General Considerations on the Current State of the Art

At both national and international levels, various models of linear electromagnetic actuators with permanent magnets have been developed, each with different structural designs and mechanical performance levels.

Depending on the dimensions of the actuators and the materials used in their construction, devices have been created that can generate forces ranging from 1–10 N up to kN [3].

Electromagnetic actuators with permanent magnets are designed to meet specific performance requirements from the design stage, such as the force developed at maximum and minimum air gaps, the stroke of the mobile armature, the total volume, mass, etc.

## 2.2. Structural Solutions for Electromagnetic Actuators Developed So Far

### The First Model of Electromagnetic Actuator with Permanent Magnets

The first model of electromagnetic actuator with permanent magnets presented in the State of the Art features a relatively simple construction, symmetrical in both longitudinal and transversal planes, as shown in the following figure:

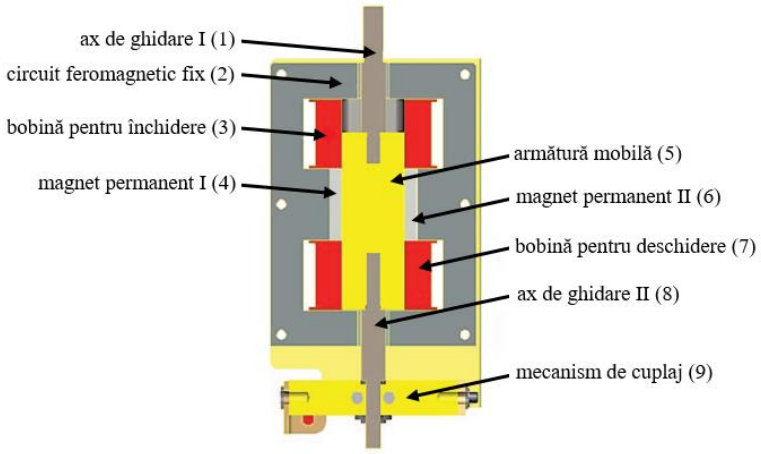


Fig. 2.1. Conceptual drawing of the first electromagnetic actuator model with permanent magnets from the current state of the art [4]

The main components of this actuator are: guide rods I and II (1 and 8), fixed ferromagnetic circuit (2), closing coil (3), permanent magnets I and II (4 and 6), mobile armature (5), opening coil (7), and coupling mechanism (9), as described in [4].

The magnetic field sources are the permanent magnets I and II (4 and 6), the closing coil (3), and the opening coil (7). These components generate the magnetic field required for actuator's operation in the two resting positions and during the closing and opening maneuvers, as illustrated in Figure 2.2.

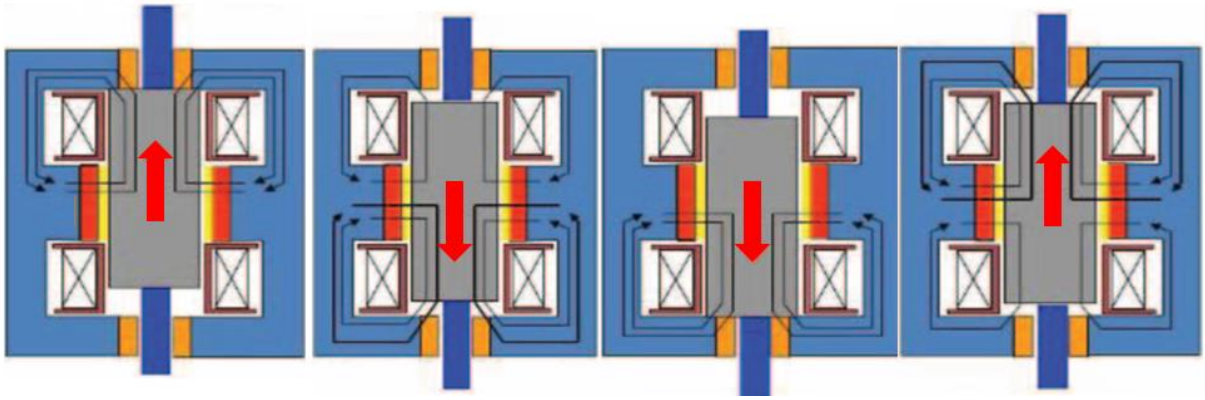

(a) (b) (c) (d)

Fig. 2.2. Magnetic field circulation within the actuator's magnetic circuit in: (a) first resting position, (b) during closing maneuver, (c) at the end of closing, and (d) during opening [4]

This actuator model presents several disadvantages, including the presence of two separate coils (one for closing maneuver and one for opening maneuver), and a limited stroke of the mobile armature due to the geometry of the fixed ferromagnetic circuit.

**The Second Model of Electromagnetic Actuator with Permanent Magnets**

The second actuator model consists of two distinct parts within the same enclosure: the actuation part, represented by a classical solenoid with a plunger, and the magnetic latching and opening part, as shown in the Fig. 2.3.

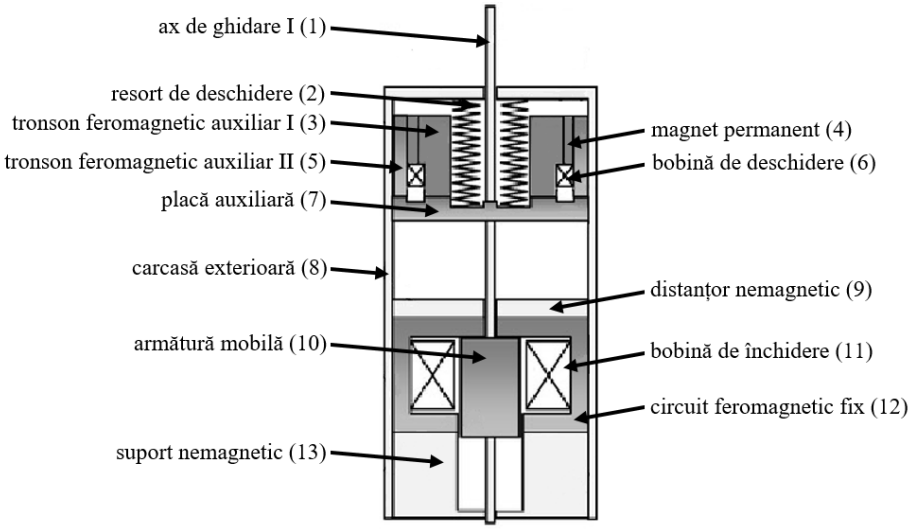


Fig. 2.3. Conceptual drawing of the second electromagnetic actuator model with permanent magnets (in upper resting position) from the current state of the art [5]

Functionally, the structure can be divided into two parts as presented in [5]. The actuation part comprises the fixed ferromagnetic circuit (12), mobile armature (10), and closing coil (11), mounted on a non-magnetic support (13). The magnetic latching and opening subassembly includes auxiliary

ferromagnetic plates I (3) and II (5), opening spring (2), permanent magnet (4), opening coil (6), and auxiliary plate (7).

Both parts are enclosed within an external casing (8), separated by a non-magnetic spacer (9). Guide rod I (1) is mechanically connected to both the mobile armature (10) and the auxiliary plate (7), so that force applied to one component is transferred to the other.

.The drawbacks of this design include the need for two coils and a relatively large overall actuator length, since all components are aligned along the guide rod. The high number of components also reduces overall reliability and lifespan.

**The Third Model of Electromagnetic Actuator with Permanent Magnets**

The third model features an axisymmetric design [6], incorporating technological aspects not found in the previous solutions.

Its main parts include: fixed ferromagnetic circuit, mobile ferromagnetic circuit, excitation coil, and two auxiliary ferromagnetic circuits, as shown in Figure 2.4.

The fixed ferromagnetic circuit consists of the upper (2), lateral (6), and lower (9) plates. The mobile armature is composed of the guide rod (1), central column (10), and pole segment (11). At the top, beneath the upper plate (2), is the upper auxiliary circuit (plate 4 and permanent magnet I (3)). The lower auxiliary circuit (plate 7 and permanent magnet II (8)) is located above the lower plate (9).

Although similar in operating principle to the previous designs, this model introduces a key innovation: during the upper resting position, magnetic flux is distributed through both the air gap between central column (10) and upper plate (2), and also in the air gap between pole segment (11) and lower plate (9).

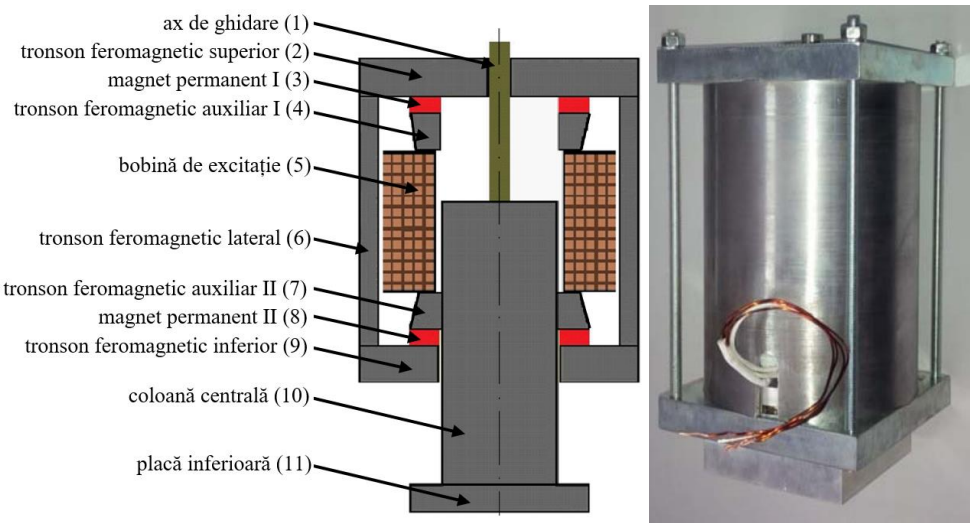


(a) (b)

Fig. 2.4. Conceptual drawing (a) and experimental model (b) of the third electromagnetic actuator with permanent magnets [6]

In the first resting position, the coil is not energized and the magnetic field is generated exclusively by the permanent magnets. The magnetic flux density in the air gap between central column (10) and upper plate (2) is negligible, resulting in a weak force, insufficient to move the armature.

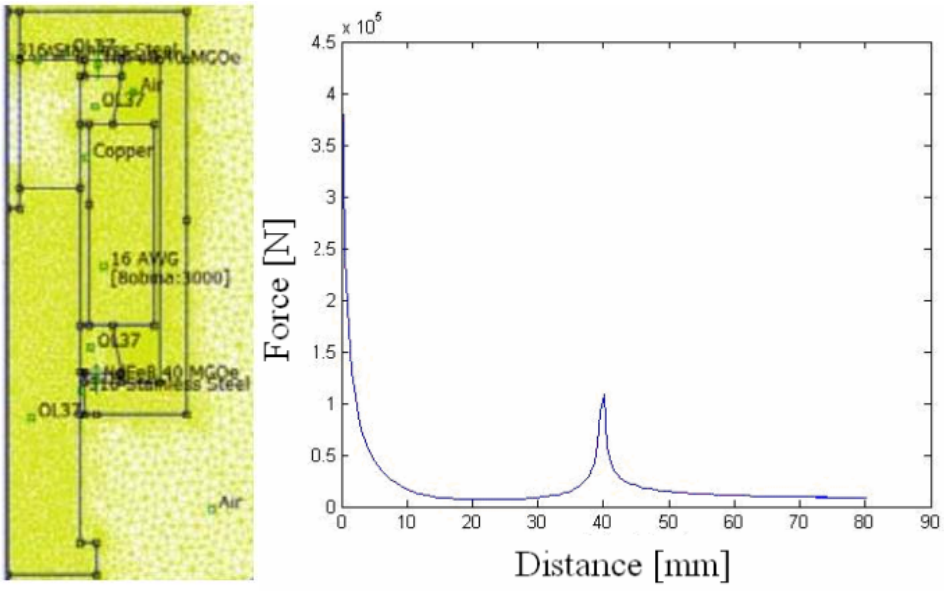


(a) (b)

Fig. 2.5. Numerical modeling (a) and force versus air gap plot during closing maneuver (b) for the third model of electromagnetic actuator [6]

This design suffers from magnetic leakage and flux dispersion due to the proximity of the upper auxiliary circuit to the lateral plate, leading to reduced force during the closing maneuver as seen in Fig. 2.5.

**The Fourth Model of Electromagnetic Actuator with Permanent Magnets**

The fourth model has a relatively simple, symmetric structure along its axis of symmetry, as illustrated in Figure 2.6.

Its main components include: fixed ferromagnetic circuit, mobile armature (2), two excitation coils (3), and auxiliary ferromagnetic circuit [7]. The fixed circuit consists of the upper (1) and lateral (4) ferromagnetic plates, while the auxiliary circuit comprises plates I (5), II (7), and permanent magnets (6).

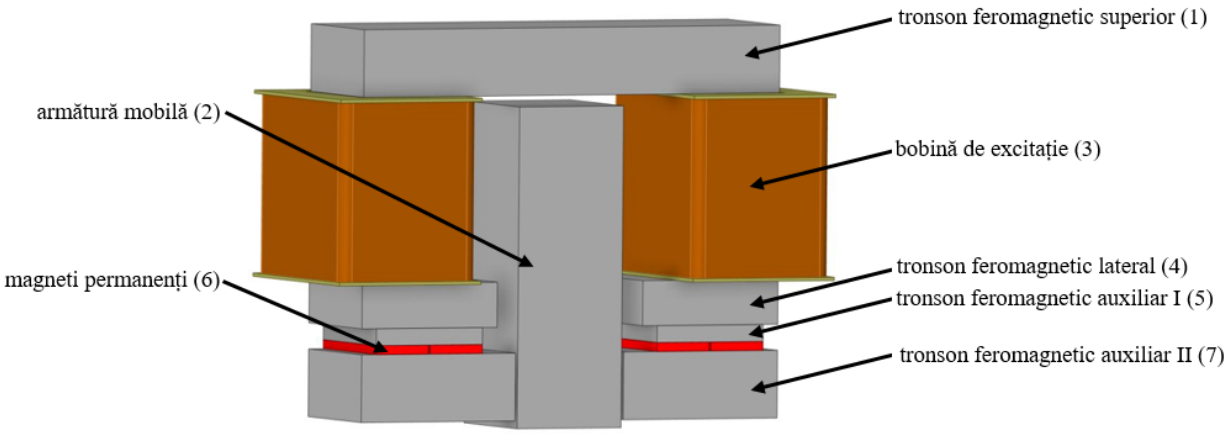


Fig. 2.6. Conceptual drawing of the fourth model of electromagnetic actuator with permanent magnets from the current state of the art [7]

## The Fifth Model of Electromagnetic Actuator with Permanent Magnets

The fifth model differs from previous designs. Unlike the second solution, where permanent magnets are located inside the actuator's enclosure, this version is composed of two distinct subassemblies: the magnetic latching mechanism and the actuation subassembly, as shown in Fig. 2.7.

Fig. 2.7. Conceptual drawing of the fifth model of electromagnetic actuator with permanent magnets from the current state of the art [8]

The actuation subassembly (lower part) includes the fixed ferromagnetic circuit (9), mobile armature (13), closing (10) and opening (12) coils, and non-magnetic spacer II (11)..

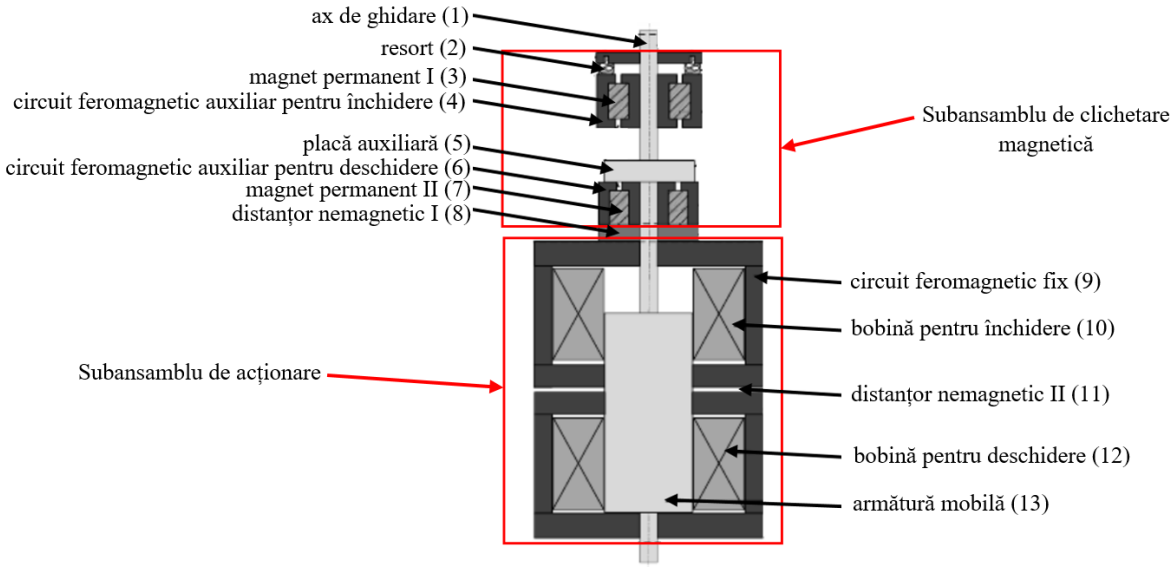


The magnetic latching subassembly consists of two auxiliary ferromagnetic circuits—one for closing (4) and one for opening (6)—each containing permanent magnets I (3) and II (7), and

between them is the auxiliary ferromagnetic plate (5) [8]. The spring (2), used during opening, is placed in the closing auxiliary circuit

The two subassemblies are separated by the non-magnetic spacer I (8), and the kinetic energy of the mobile armature (13) is transmitted to the auxiliary plate (5) via the guide rod (1), as shown in Figure 2.8..

.

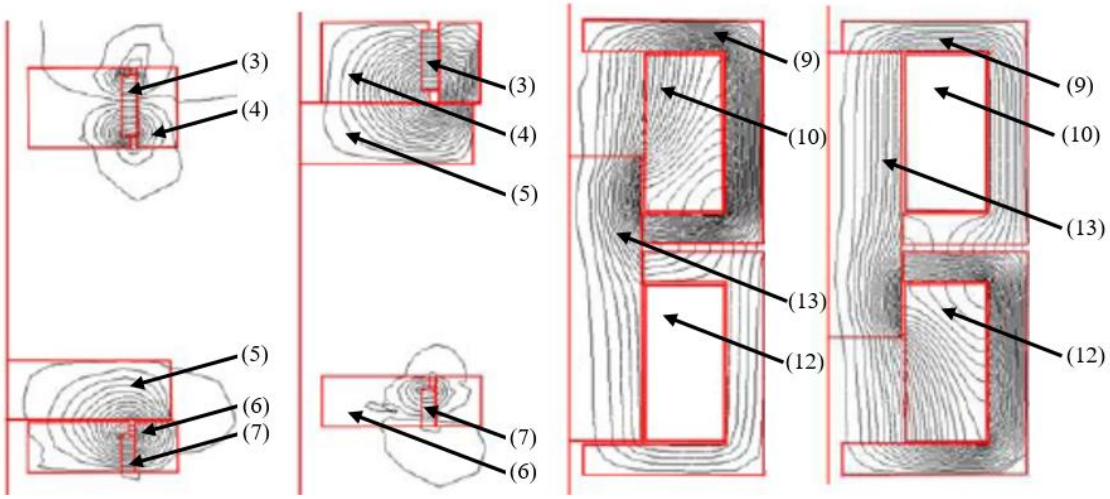


Fig. 2.8. Magnetic field inside actuator's subassemblies during: (a) first resting position, (b) second resting position, (c) closing maneuver, (d) opening maneuver [8]

The disadvantage of this solution lies in the high number of components, which negatively affects reliability and durability.

# 3. Development of a New Model of Electromagnetic Actuator with Permanent Magnets

## 3.1. General Considerations for the new model of Electromagnetic Actuator with Permanent Magnets

The developed linear electromagnetic actuator includes a fixed ferromagnetic circuit, an auxiliary ferromagnetic circuit, two permanent magnets, an excitation coil, and a mobile ferromagnetic armature (also referred to in the thesis as a mobile ferromagnetic circuit) [9], configured as a plunger, as can be seen in the following figure:

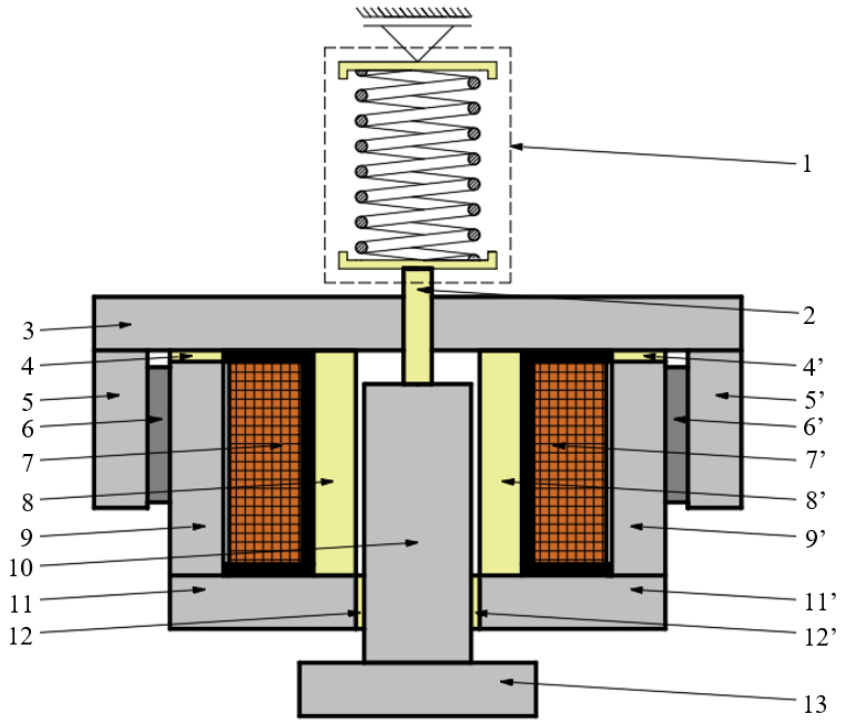


Fig. 3.1. Sectional view of the first model of electromagnetic actuator with highlighted main components [9]

The main components of the electromagnetic actuator are as follows: 1 – spring-based opening mechanism; 2 – striker; 3 – upper ferromagnetic plate; 4, 4' – upper spacers; 5, 5' – auxiliary ferromagnetic plate; 6, 6' – permanent magnets; 7, 7' – excitation coil; 8, 8' – inner supports; 9, 9' – lateral ferromagnetic plates; 10 – central column; 11, 11' – lower ferromagnetic plates; 12, 12' – lower spacers; 13 – pole segment.

## 3.2. Operating principle of the linear electromagnetic actuator with permanent magnets

### 3.2.1. Similarities and differences with classical structural solutions

The linear electromagnetic actuator with permanent magnets developed in this thesis operates on a principle similar to that of a classical electromagnet. The purpose of the device is to generate an electromagnetic force that displaces the mobile armature relative to the fixed one, effectively reducing the air gap between them.

Unlike a classical electromagnet, which requires continuous power supply to generate a usable force, the developed linear actuator is capable of exerting magnetic force at minimum air gap without consuming electrical energy. This is due to the permanent magnets included in the structure, which generate a static magnetic field directed towards the air gap by means of the auxiliary magnetic circuit.

### 3.2.2. Operating positions of the linear electromagnetic actuator

#### 3.2.2.1. General considerations regarding the operating positions of the linear electromagnetic actuator with permanent magnets

Regarding the operating principle, four states of the actuator can be defined based on the position of the mobile armature (as shown in Figure 3.1) and the power supply status of the excitation coil, as follows:

- the actuator is open, and the coil is not energized (resting position with maximum air gap), in which the device remains open without electrical energy consumption;
- the actuator is open, and the coil is energized for closing (referred to as latching or closing maneuver);
- the actuator is closed, and the excitation coil is not energized (resting position with minimum air gap), in which the device remains closed without electrical energy consumption;
- the actuator is closed, and the coil is energized for opening (referred to as tripping or opening maneuver).

#### 3.2.2.2. Resting Position at Maximum Air Gap

In the resting position at maximum air gap, the spring is pre-compressed and exerts a stabilizing force that ensures the actuator remains open, even if an accidental force is applied in the closing direction. In this resting position, with the actuator open, the air gap has a maximum value of $\delta_{max}$ [mm], and the spring is compressed by k [mm]. The opening spring exerts a pre-compression force $\overline{F}_{res,k}$ [N] on surface $S_1$, without being further compressed, and thus remains in its initial position inside the mechanism, as shown in Figure 3.2.

In this operating state, the mechanical equation can be written as follows:

$$\vec{G} + \vec{F}_{res,k} + \vec{F}_{r_1} = 0 \quad (3.1)$$

where $\vec{G}$ is the weight of the mobile components, and $\vec{F}_{r_1}$ is the reaction force, equal in magnitude and opposite in sign to the sum of the other two forces, acting on surface $S_1$; considering the direction of the forces, the previous equation becomes:

$$G + F_{res,k} - F_{r_1} = 0 \quad (3.2)$$

#### 3.2.2.3. Closing Maneuver

During the actuator's closing maneuver, both the force generated by the actuator and the force developed by the opening spring increase. In order to complete the closing maneuver—i.e., to reduce the air gap between the mobile and fixed armatures—the electromagnetic actuator must generate a force greater than the opposing (antagonistic) force resisting the movement. This can be mathematically expressed as:

$$|\vec{F}_e| > |\vec{F}_{res,k}| + |\vec{G}| \quad (3.3)$$

where $\vec{F}_e$ [N] is the force developed by the actuator for a given air gap $\delta$ [mm], $\vec{F}_{res,k}$ [N] is the force exerted by the opening spring corresponding to that air gap, and $\vec{G}$ is the weight of the mobile armature, all illustrated in Figure 3.2.

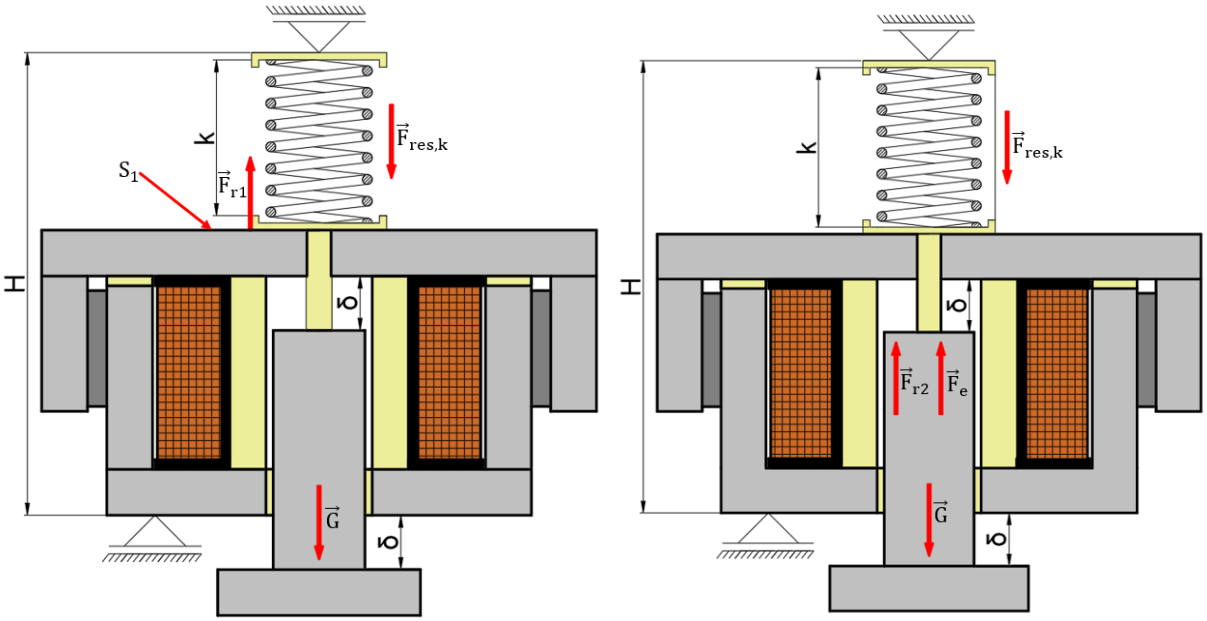


Fig. 3.2. Representation of the forces acting in the resting position (left) at maximum air gap and during the latching maneuver (right)

### 3.2.2.4. Resting Position at Minimum Air Gap

In the resting position at minimum air gap, after the latching maneuver has been completed, the mobile armature must be held in the closed position. To achieve this, the holding force generated by the permanent magnets must be greater than the sum of all opposing forces:

$$|\vec{F}_e| > |\vec{F}_{res,k-\delta}| + |\vec{G}| \qquad (3.4)$$

where $\vec{F}_e$ [N] is the electromagnetic holding force developed by the actuator while it is in the resting position at minimum air gap—this force being generated solely by the permanent magnets; $\vec{F}_{res,k-\delta}$ [N] is the force exerted by the opening spring when it is compressed by $k - \delta$ [mm], and $\vec{G}$ [N] is the weight of the moving components, as shown in Figure 3.3.

### 3.2.2.5. Opening Maneuver

During the opening maneuver, the actuator initially has a minimum air gap, and the excitation coil is energized such that the magnetic flux generated by it is in the opposite direction to that produced by the permanent magnets, relative to the magnetic circuit. A resultant magnetic field is generated in the actuator, composed of the magnetic field from the coil and that from the permanent magnets. The magnetic flux density in the air gap becomes negligible, which leads to a weak electromagnetic force that can be neglected in the force system equation.

Since the electromagnetic force produced by the actuator is negligible, the opposing forces that now lead to its opening, i.e., to the separation of the mobile armature from the fixed one.. The two forces responsible for this movement are the weight of the mobile armature $\vec{G}$ and the force

$\vec{F}_{res,k-\delta}$, exerted by the opening spring, which has an elongation of $k - \delta$ at the beginning of the tripping maneuver, as illustrated in Figure 3.3.

From a mechanical perspective, the tripping maneuver of the electromagnetic actuator can be expressed in vectorial form as follows:

$$\vec{G} + \vec{F}_{res,k-\delta} = \vec{F}_{r4} \qquad (3.5)$$

where $\vec{F}_{r4}$ is the resultant force during the opening process and is directly proportional to the mass of the moving components and the acceleration acquired by the mobile armature during this maneuver.

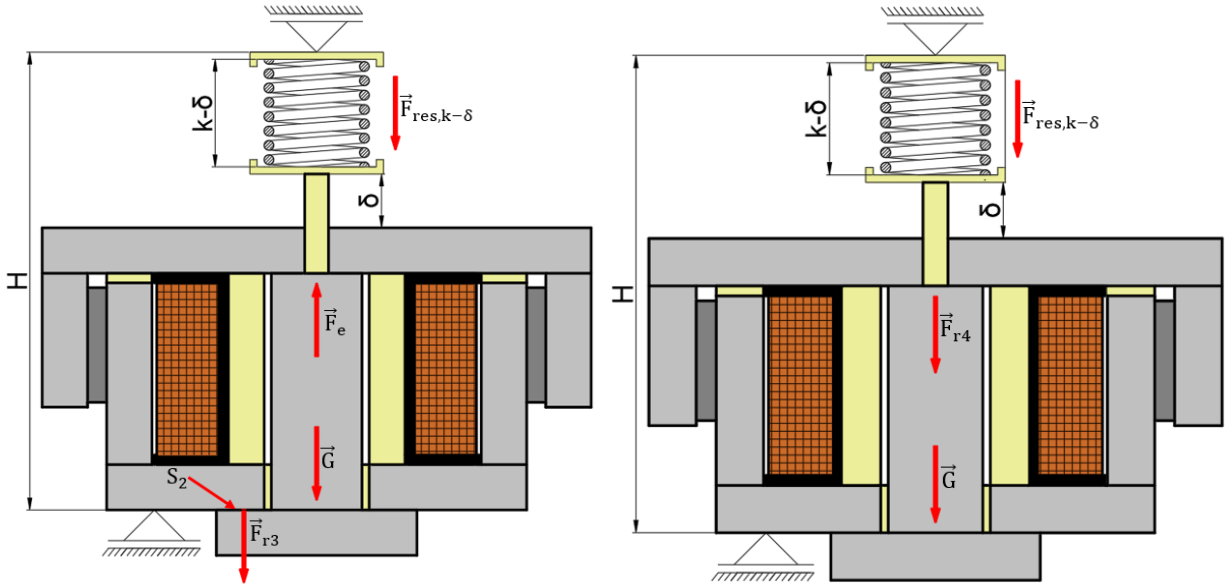


Fig. 3.3. Representation of the forces in the resting position at minimum air gap (left) and during the opening maneuver (right)

## 4. Analytical Computation of the Electromagnetic Actuator with permanent magnets components

The analytical sizing of the subassemblies of the electromagnetic actuator involves determining certain geometric dimensions for each of its components, as well as establishing the electromagnetic parameters that govern the device's operation.

The computation of the actuator's main dimensions was based on specific performance criteria, dimensional constraints, and technical limitations, including:

- the maximum air gap between the mobile and fixed armature is $\delta_{max} = 22$ mm;
- the force generated by the electromagnet at maximum air gap is $F_{\delta_{max}} = 4900$ N;
- the maximum flux density in the sections of the ferromagnetic circuit does not exceed $B_{max} = 1.6$ T.

To dimension the electromagnetic actuator so that it can generate the required latching force, it must be considered that it has two magnetic field sources: the excitation coil and the permanent magnets integrated into the structure.

An approximate model for computing the magnetic field within the actuator is the magnetic circuit model. Since magnetic field problems are complex, this thesis places particular emphasis on numerically determining the solution of the electromagnetic field using a specialized finite element method software.

Given that the magnetic flux can travel through the magnetic plates both longitudinally and transversely, it is necessary to model their reluctance depending on the magnetic field's direction of propagation. Both the permanent magnets and the excitation coil are modeled as magnetic field sources, each generating a certain magnetomotive force; a similar modeling approach is found in [10].

To analyze the reluctances within the actuator's magnetic circuit, they are modeled both by circuit segment and by the orientation of magnetic flux through them, as seen in [11].

The equivalent magnetic circuit includes the following components:

- $R_1$, $R_2$, $R_3$, $R_4$, $R_5$, $R'_1$, $R'_2$, $R'_3$, $R'_4$, $R'_5$, $R_6$ – reluctances in the upper ferromagnetic plate;
- $R_7$, $R_{11}$, $R'_7$, $R'_{11}$ – reluctances in the auxiliary ferromagnetic plates;
- $R_9$, $R_{13}$, $R_{14}$, $R'_9$, $R'_{13}$, $R'_{14}$ – reluctances in the lateral ferromagnetic plates;;
- $R_{15}$, $R_{17}$, $R_{18}$, $R_{21}$, $R'_{15}$, $R'_{17}$, $R'_{18}$, $R'_{21}$ – reluctances in the lower ferromagnetic plates;
- $R_{16}$, $R_{20}$, $R'_{20}$, $R_{23}$ – reluctances in the central column;
- $R_{24}$, $R'_{24}$, $R_{25}$, $R_{26}$, $R'_{26}$ – reluctances in the pole segment;
- $R_{12}$, $R'_{12}$ – reluctances of the permanent magnets;
- $R_{10}$ – the air gap reluctance formed between the central column and the upper ferromagnetic plate (variable according to the position of the mobile ferromagnetic circuit);;
- $R_{22}$, $R'_{22}$ – air gap reluctances formed between the pole segment and the lower ferromagnetic plates (also variable with the position of the mobile ferromagnetic circuit);

- $R_8$, $R'_8$ – magnetic reluctance of the air gap formed between the lateral and upper ferromagnetic plates;;
- $R_{19}$, $R'_{19}$ – magnetic reluctance of the air gap between the lower ferromagnetic plate and the central column;
- $R_D$, $R'_D$ – magnetic reluctance through which the flux generated by the permanent magnets disperses;
- $u_{mg,MP}$ – magnetomotive force generated by a permanent magnet;
- $u_{mg,B}$ – magnetomotive force generated by the excitation coil.

Considering the reluctance modeling of the actuator's magnetic circuit, the equivalent schematic presented in **Figure 4.1** can be constructed, which includes the magnetic field sources.

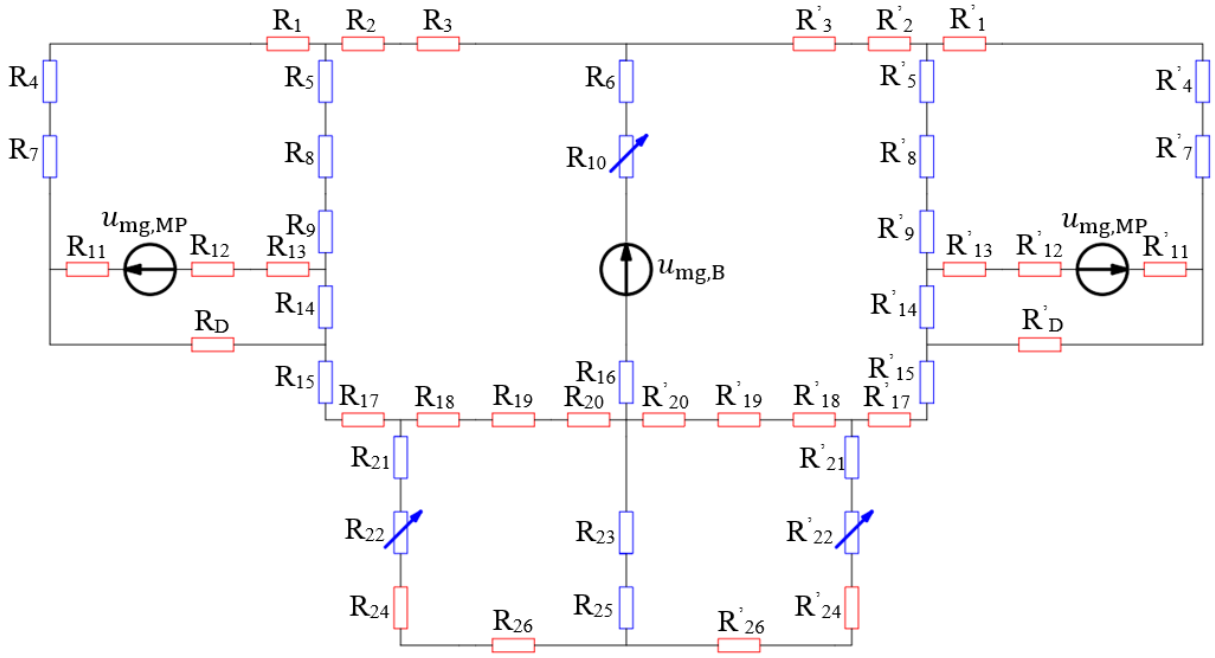


Fig. 4.1. Equivalent magnetic circuit model of the electromagnetic actuator, considering the magnetic flux orientation through the ferromagnetic plates

At maximum air gap, it can be assumed that the equivalent reluctance of the magnetic circuit is approximately equal to the reluctance of the air gaps traversed by the magnetic flux, that is:

$$R_{ech} \approx R_{întrefier} \qquad (4.1)$$

Neglecting stray magnetic fields, the magnetic flux through the air gap during closing maneuver (i.e., at maximum air gap) can be approximated by the following relation:

$$\varphi_{ancl} = \frac{\theta_{bobină}}{R_{întrefier}} = \frac{\theta_{bobină}}{\frac{L_{k,ech}}{\mu_0 A_{k,ech}}} = \frac{\mu_0 \theta_{bobină} A_{k,ech}}{L_{k,ech}} \qquad (4.2)$$

where $\theta_{bobină}$[A] is the magnetomotive force generated by the coil.

Accordingly, the magnetic flux density in the air gap during closing maneuver can be approximated as:

$$B_{ancl} = \frac{\varphi_{ancl}}{A_{k,ech}} = \frac{\mu_0 \theta_{bobină}}{L_{k,ech}} \qquad (4.3) \quad [12]$$

where $B_{ancl}$ [T] is the magnetic flux density in the main air gap during the closing operation (i.e., the gap between the central core and the ferromagnetic section), and $\varphi_{ancl}$[Wb] is the magnetic flux through its cross-sectional area. The force can be approximated using the following formula:

$$F_{\delta_{max}} = \frac{B_{ancl}^2 A_c}{2\mu_0} = \frac{\varphi_{ancl}^2}{2\mu_0 A_c} \quad (4.4) \quad [12][13]$$

where $A_c$ is the cross-sectional area of the air gap between the central column and the upper ferromagnetic plate. Considering the magnetic flux expression, the developed force at closing maneuver can be rewritten as:

$$F_{\delta_{max}} = \frac{\left(\frac{\mu_0 \theta_{bobină} A_{k,ech}}{L_{k,ech}}\right)^2}{2\mu_0 A_c} = \frac{\mu_0 A_{k,ech} \theta_{bobină}^2}{2L_k^2} \quad (4.5)$$

From equation (4.3), the required magnetomotive force to produce a specific magnetic flux density in the air gap can be computed:

$$\theta_{bobină} = \frac{B_{ancl} L_{k,ech}}{\mu_0} \qquad (4.6)$$

Considering the equivalent length of the air gap as approximately 29 mm and that the magnetic flux density in the gap should not exceed the saturation point of the ferromagnetic circuit (i.e. $B_{ancl} \cong 1.6$ T), the magnetomotive force is:

$$\theta_{bobină} = \frac{1.6 \cdot 0.029}{4\pi \cdot 10^{-7}} = 36900 \text{ Asp} \qquad (4.7)$$

Including a safety margin of 8–10%, the magnetomotive force produced by the coil is approximately $\theta_{bobină} = 40$ kAsp.

From equation (4.5), the area through which the magnetic flux flows can be determined using the known mechanical and electromagnetic parameters is:

$$A_{k,ech} = \frac{2L_k^2 F_{\delta_{max}}}{\mu_0 \theta_{bobină}^2} = \frac{2 \cdot 0.029^2 \cdot 4900}{4\pi \cdot 10^{-7} \cdot 40000^2} = 4.1 \cdot 10^{-3} \text{m}^2 \qquad (4.8)$$

The magnetic flux through the air gap at closing maneuver can be computed using equation (4.2):

$$\varphi_{ancl} = \frac{\mu_0 \theta_{bobină} A_{k,ech}}{L_{k,ech}} = \frac{4\pi \cdot 10^{-7} \cdot 40000 \cdot 4.5 \cdot 10^{-3}}{0.029} = 7.8 \text{ mWb} \qquad (4.9)$$

To maintain optimal proportions between the geometric dimensions of the device, the central column is designed from solid steel with a cross-section of 120 mm × 38 mm, while the other plates of the ferromagnetic circuit are made of solid steel with a 120 mm × 19 mm cross-section, where 120 mm corresponds to the depth of the electromagnetic actuator.

Since the coil must generate the magnetic field required for the actuator's operation, the main design parameter is the magnetomotive force that ensures nominal functioning, i.e., $\theta = 40$ kAsp. Assuming a preliminary current density in the coil section of $J_p = 25 A/mm^2$, the cross section area (including the housing) is: $A_b = 1600\ mm^2$.

If a 10% space reserve is considered, the height of the winding is:

$$h_b = 0.9 \cdot \left(h_{tronson,lateral} + l_{distanțor}\right) - 2g \quad (4.10)$$

Considering that the maximum height of the section into which the coil can be inserted is 80 mm, it follows that the winding height is: $h_b = 0.9 \cdot 80 - 2 \cdot 4 = 64$ mm.

Taking into account that the entire cross section of the coil is known and that it is equal to the product of the winding height and its thickness, it results that the winding thickness is:

$$g_b = \frac{A_b}{h_b} - g = \frac{1600}{64} - 4 = 25 \text{ mm} \quad (4.11)$$

Taking into account the housing thickness (i.e. 2 mm) the total winding thickness is 27 mm.

To determine the electrical parameters, it is necessary to compute the average turn length of the coil, which is illustrated in the following figure:

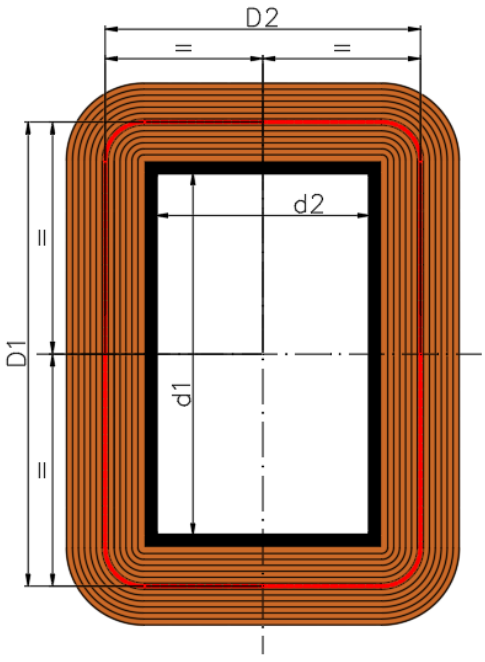


Fig. 4.2. Regarding the average turn length of the coil of the electromagnetic actuator

By analyzing Figure 4.2, the average length of a turn can be determined, which depends on the dimensions of the central column of the fixed armature, the thickness of the coil housing, and its other general dimensions, respectively:

$$l_{spmed} \cong 2 \cdot D1 + 2 \cdot D2 = 2\,(d1 + g_b + 2g) + 2(d2 + g_b + 2g) = 2 \cdot d1 + 2 \cdot d2 + 4g_b + 8g$$

$$\rightarrow l_{spmed} = 2 \cdot 122 + 2 \cdot 74 + 4 \cdot 27 + 8 \cdot 4 \rightarrow l_{spmed} \cong 532\ \text{mm} = 0.532\ \text{m} \quad (4.12)$$

The cross-sectional area of the conductor can be computed using the following relation:

$$S_{cond} = \frac{\pi d_{neiz}^2}{4} = \frac{\pi(d_{iz} - g_{iz})^2}{4} \quad (4.13)$$

where $d_{neiz}$ is the diameter of the copper conductor without insulation, $g_{iz}$ este grosimea izolației, is the thickness of the insulation (i.e., the enamel layer), and $d_{iz} = d_{iz} + g_{iz}$ is the diameter of the conductor with insulation.

The resistance of the coil can be expressed as:

$$R_b = \frac{4 \cdot \rho_{Cu} \cdot A_b \cdot l_{spmed}}{\pi(d_{iz} - g_{iz})^2 d_{iz}^2} \quad (4.14)$$

From the magnetic circuit law, the preliminary electric current circulating through the winding can be determined, considering the number of turns and the magnetomotive force produced by the coil:

$$I_b = \frac{\theta_{bobină} \cdot d_{iz}^2}{A_b} \quad (4.15)$$

Given that both the current and the electrical resistance of the coil are known, the voltage at its terminals can be determined using relations (4.14) and (4.15):

$$U_b = R_b \cdot I_b = \frac{4 \cdot \rho_{Cu} \cdot A_b \cdot l_{spmed}}{\pi(d_{iz} - g_{iz})^2 d_{iz}^2} \cdot \frac{\theta_{bobină} \cdot d_{iz}^2}{A_b} \rightarrow U_b = \frac{4 \cdot \rho_{Cu} \cdot \theta_{bobină} \cdot l_{spmed}}{\pi \cdot (d_{iz} - g_{iz})^2} \quad (4.16)$$

Since both the applied voltage at the coil terminals and the magnetomotive force produced are known, the diameter of the conductor can be determined:

$$d_{neiz} = d_{iz} - g_{iz} = \sqrt{\frac{4 \cdot \rho_{Cu} \cdot \theta_{bobină} \cdot l_{spmed}}{\pi \cdot U_b}} \quad (4.17)$$

Substituting numerical values yields to:

$$d_{neiz} = \sqrt{\frac{4 \cdot 1.724 \cdot 10^{-8} \cdot 40 \cdot 10^3 \cdot 0.532}{\pi \cdot 230}} \rightarrow d_{neiz} = 14.25 \cdot 10^{-4}\text{m} = 1.425\ \text{mm} \quad (4.18)$$

From standardized tables, choosing the next higher value, i.e. $d_{neiz} = 1.5$ mm, the enamel insulation thickness is $g_{iz} = 0.08$ mm, and the total insulated conductor diameter is $d_{iz} = 1.58\ mm$. In this case, the conductor cross-section is:

$$S_{cond} = \frac{\pi d_{neiz}^2}{4} = \frac{\pi (d_{iz} - g_{iz})^2}{4} = \frac{\pi \cdot 1.5^2}{4} = 1.767\ \text{mm}^2 = 1.767 \cdot 10^{-6}\ \text{m}^2 \quad (4.19)$$

Given that the general dimensions of the coil window are known, the number of turns can be determined considering the insulated conductor diameter and the turn layout. The number of turns per layer can be computed with:

$$N_{spire/strat} = \frac{h_b}{d_{iz}} = \frac{64}{1.58} \rightarrow N_{spire/strat} = 40\ \text{turns/layer} \quad (4.20)$$

The total number of layers can similarly be computed, taking into account the insulated diameter and turn layout:

$$N_{straturi} = \frac{g_b}{d_{iz}} = \frac{27}{1.58} \rightarrow N_{straturi} = 17\ \text{layers} \quad (4.21)$$

Considering the two quantities determined above, the total number of turns can be computed as:

$$N_{spire} = N_{spire/strat} \cdot N_{straturi} = 40 \cdot 17 \rightarrow N_{spire} = 680\ \text{turns} \quad (4.22)$$

The electrical resistance can be computed considering the number of turns, the average turn length, and the conductor cross-section:

$$R_b = \frac{\rho \cdot N_{spire} \cdot l_{spmed}}{S_{cond}} = \frac{1.724 \cdot 10^{-8} \cdot 680 \cdot 0.532}{1.767 \cdot 10^{-6}} \rightarrow R_b = 3.53\ \Omega \quad (4.23)$$

The electric current flowing through the coil can be computed considering the rated voltage at its terminals and the electrical resistance:

$$I_b = \frac{U_b}{R_b} = \frac{230}{3.53} \rightarrow I_b = 65.16\ \text{A} \quad (4.24)$$

The magnetomotive force (MMF) produced by the coil during energizing can be determined based on the number of turns and current:

$$\theta_{bobină} = N \cdot I_b = 680 \cdot 65.16 \rightarrow \theta_{bobină} = 44300\ \text{Asp} \quad (4.25)$$

The obtained value for MMF is approximately 10% higher than the one determined analytically during the magnetic circuit design and the estimation of electromagnetic parameters, i.e. 40 kAt. Regarding this, if a 10% reduction in voltage at the coil terminals is considered (as specific to low-voltage power networks), the produced MMF is approximately equal to the required one.

# 5. Numerical Modeling of the current – fed Electromagnetic Actuator

## 5.1. General Considerations

The analysis of the electromagnetic actuator model consists in studying the operation of the device regarding electromagnetic phenomena in the two resting positions, as well as during switching (closing and opening) operations.

Evidently, in order to explain the operation of the electromagnetic actuator, it is necessary to highlight the influence of electromagnetic parameters, as well as kinematic parameters.

In this regard, to study the influence of geometrical dimensions on both kinematic and electromagnetic parameters, a 2D numerical model of the actuator was implemented using the finite element software FEMM [14]. The implemented problem is of the planar-parallel type, with a model depth of 120 mm, and the frequency imposed in the numerical model is zero. Thus, the analysis of the electromagnetic actuator can be carried out considering a steady-state magnetic field regime.

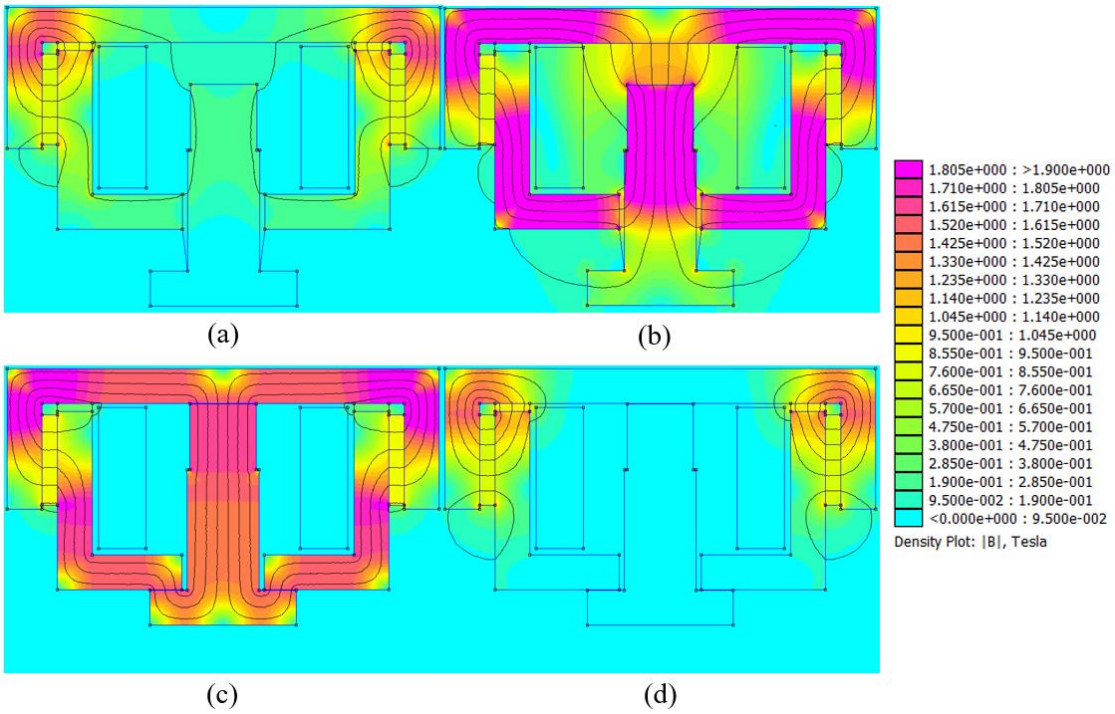


Fig. 5.1. Magnetic field within the magnetic circuit of the actuator in its four operating states: resting position with maximum air gap (a), closing maneuver (b), resting position with minimum air gap (c), and opening maneuver (d)

As can be seen in the above figure, the magnetic flux tends to traverse all the reluctances of the ferromagnetic circuit depending on the operating position. In order to explain the influence of geometric and electromagnetic parameters on the force developed by the actuator, the analysis starts from Kirchhoff's Second Law for magnetic circuits.

The magnetic field is guided through the fixed ferromagnetic circuit, which has a geometry allowing the circulation of field lines through both the main and auxiliary plates. It should also be noted that the mobile armature includes at its lower part the pole segment (13) (highlighted in Fig.

3.1), which serves to direct the magnetic field at minimum air gap. The geometric shape of the mobile armature allows the magnetic flux to circulate through a larger surface area, unlike a conventional electromagnet, where the magnetic field is strictly guided through the central column.

In a conventional electromagnet, the holding force depends on the surface of the air gap defined by the central column (10) and the upper ferromagnetic plates (3), as well as on the magnetic flux through it. In the case of the newly developed actuator, the flux produced by the permanent magnets circulates through three distinct surfaces.

Increasing the effective surface of the mobile armature in this manner is achieved with minimal material consumption, and the overall dimensions of the fixed ferromagnetic circuit remain unchanged, which constitutes a novelty in the design of electromagnetic actuators with permanent magnets.

## 5.2.Modeling the Electromagnetic Actuator in its Four Operating Positions

### 5.2.1.Resting Position at Maximum Air Gap

In the resting position at maximum air gap, the actuator is open and not energized. The actuator coil is not fed with current, and therefore the magnetic field it would produce is zero. Since the actuator does not consume electrical energy, it is considered to be in a resting state.

During this position, the magnetic field is produced solely by the permanent magnets located on the fixed ferromagnetic circuit, as illustrated in the figure below:

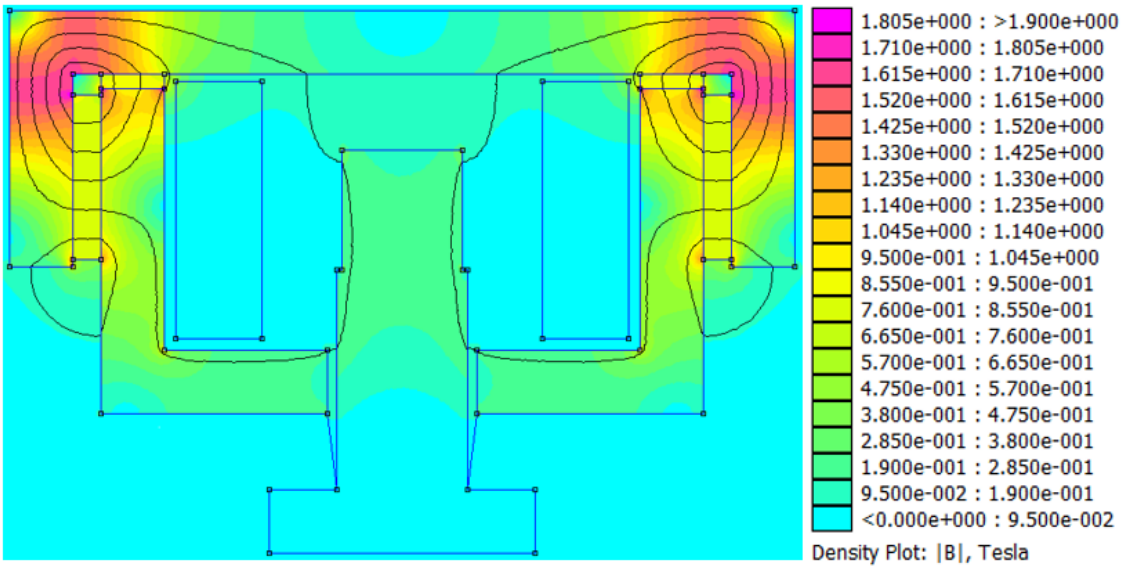


Fig. 5.2. Circulation of the magnetic field within the actuator's magnetic circuit in the open resting position

In this operating position, the magnetic field produced by the permanent magnets is directed such that the magnetic flux density in the functional air gap between the mobile and fixed armatures has a low value (on the order of mT), so that the force developed by the actuator in this state is negligible.

For this operating position, the actuator produces a low-value electromagnetic force, which depends on the average magnetic flux density in the air gap found between the mobile and fixed armatures.

The opening springs exert a relatively small force, specifically the pre-compression force $F_{res,k}$, which is necessary to maintain the maximum distance between the fixed and mobile armatures.

### 5.2.2. Closing maneuver of the Electromagnetic Actuator

During the closing operation, the actuator has a variable air gap, starting from the maximum value $\delta_{max} = 22$ mm down to the minimum (technological) air gap. To move the mobile armature, the excitation coil is powered to produce a stationary magnetic field, whose energy is guided through the fixed, mobile, and auxiliary magnetic circuits to the air gap, where the electromagnetic force required for closing is generated, depending on specific kinematic parameters.

During this operation, the magnetic field produced by the excitation coil is oriented in the same direction as that produced by the permanent magnets in the ferromagnetic circuit.

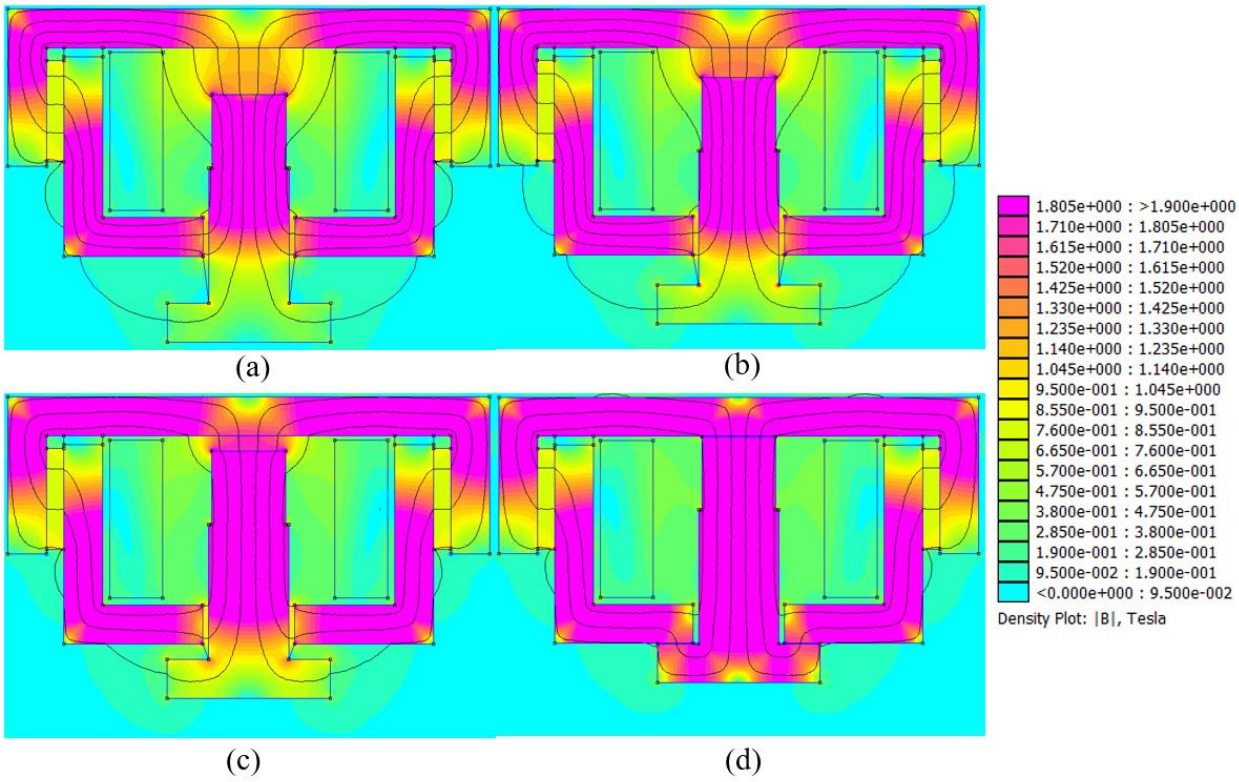


Fig. 5.3. Magnetic field within the actuator's ferromagnetic circuit and its air gap for different distances between the mobile and fixed armatures: 22 mm (a), 14 mm (b), 7 mm (c), and 0.1 mm (d)

As observed in the previous figure, during the closing maneuver, the magnetic flux tends to circulate predominantly through the air gap between the central column of the mobile armature and

the upper plate of the fixed ferromagnetic circuit, while in the area between the pole segment and the lower plates, the magnetic flux density has negligible values.

Evidently, as the magnetic flux density increases, so does the force exerted on the mobile armature [15]. Accordingly, as the mobile armature advances, the force acting upon it increases, reaching a maximum at the minimum (technological) air gap.

The attraction force between the mobile and fixed ferromagnetic circuits reduces the air gap, which leads to a decrease in magnetic reluctance. For the same current in the excitation coils and the same magnetomotive force, the magnetic flux within the magnetic circuit increases, thereby raising the magnetic flux density in the air gap.

### 5.2.3.Resting Position at Minimum Air Gap

In the closed resting position, the electromagnetic actuator has a minimum air gap, and the excitation coil is not energized, which corresponds to a resting state in which the device does not consume electrical energy. In this situation, the magnetic field is produced solely by the permanent magnets in the fixed ferromagnetic circuit.

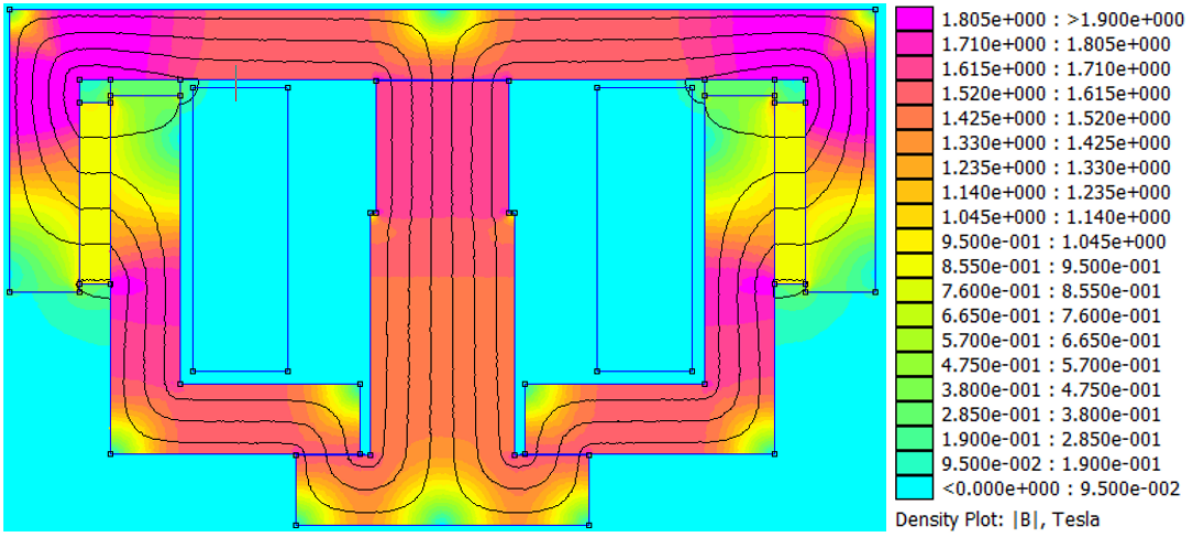


Fig. 5.4. Magnetic field circulation within the actuator's magnetic circuit during holding in the closed position

Regarding the magnetic field circulation, the electromagnetic actuator introduces a novelty compared to previously developed devices. Specifically, existing magnetic circuit designs involve a single air gap through which the magnetic flux from the permanent magnets circulates when the electromagnet is closed. The new construction solution increases the force developed by the actuator in the closed position by introducing three functional air gaps for magnetic flux circulation. This is made possible by altering the shape of the mobile armature to increase the surface area through which magnetic flux circulates.

### 5.2.4.Opening maneuver of the Electromagnetic Actuator

The opening of the electromagnetic actuator is achieved under the action of compression springs, following a reduction in the magnetic field generated by the permanent magnets.

During the opening maneuver, the excitation coil is powered and generates a magnetic field that circulates through the ferromagnetic circuit and the air gap in the opposite direction to that produced by the permanent magnets. This results in a resultant magnetic field, which depends on both the field produced by the permanent magnets and that generated by the excitation coil.

The resultant magnetic field in the magnetic circuit depends on the current through the excitation coil, as shown in Figure 5.5. According to this figure, as the current in the excitation coil increases during the opening maneuver, the magnetic field within the central column and air gap decreases. Clearly, with increasing coil current, the magnetic field generated by the coil increases, and at a certain current, it reaches a value close to that of the field produced by the permanent magnets.

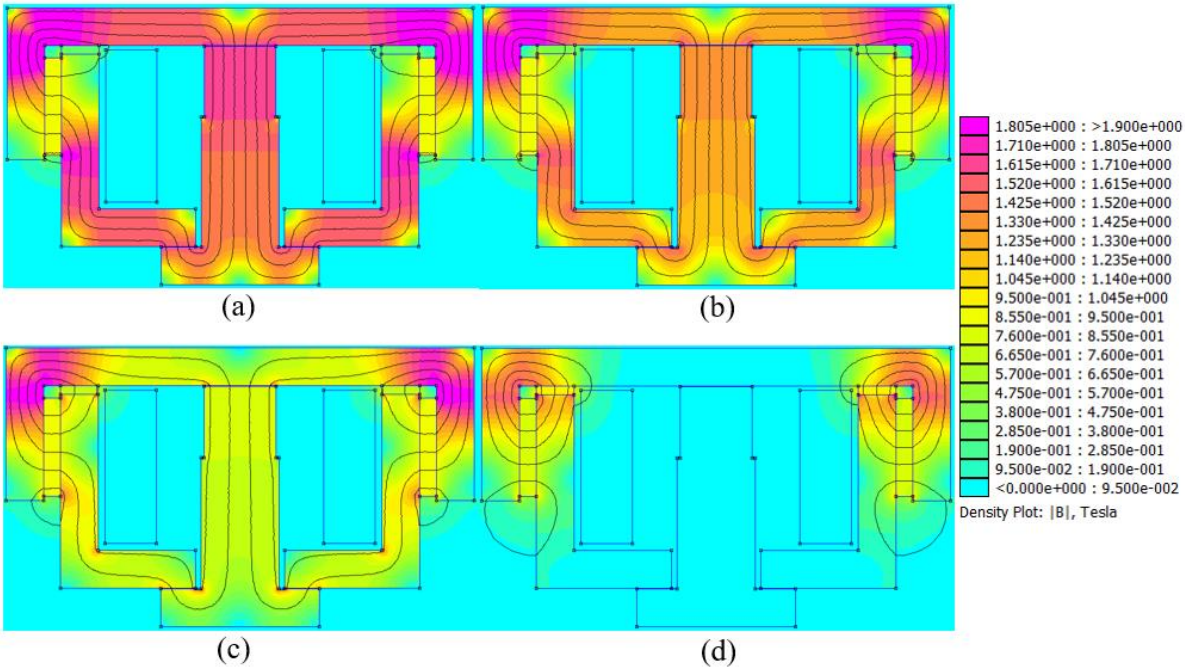


Fig. 5.5. Resultant magnetic field in the ferromagnetic circuit for various magnetomotive forces produced by the excitation coil: 0 Asp (a), 1000 Asp (b), 2000 Asp (c), and 3040 Asp (d)

Since the two magnetic fields (one generated by the coil and the other by the permanent magnets) are approximately equal and circulate through the reluctances in opposite directions [16], the resultant magnetic field through the main ferromagnetic plates becomes negligible. In this case, the electromagnetic force generated by the resultant field is smaller than the sum of antagonistic forces (namely, those generated by the opening spring and the weight of the moving parts), and as a consequence, the actuator opens.

# 6. Kinematic Analysis of the current – fed Electromagnetic Actuator

## 6.1. Kinematic Analysis of the Electromagnetic Actuator without Mechanical Load during closing maneuver

The kinematic analysis of the electromagnetic actuator without mechanical load involves determining its relevant kinematic parameters in order to establish the device's performance when operating outside the system in which it may be implemented.

Obviously, the kinematic analysis can be carried out for maneuvers in which the electromagnetic actuator consumes electrical energy and produces a certain mechanical work, specifically when the mobile armature displaces.

Considering the electromagnetic actuator uncoupled from any mechanical load (including the opening spring) during the closing maneuver, the equation of motion can be expressed as follows:

$$m \cdot \vec{a}_{ancl} + \vec{F}_e + \vec{G} = 0 \rightarrow m \cdot \vec{a}_{ancl} + \vec{F}_e + m\vec{g} = 0 \qquad (6.1)$$

where m [kg] is the mass of the moving components, $a_{ancl}$ $[m/s^2]$ is the acceleration, and $F_{elmg}$ [N] is the force generated by the electromagnetic actuator at the air gap δ; taking into account the direction of the acting forces, the equation above can be rewritten as::

$$m \cdot a_{ancl} = F_{elmg,\delta} - m \cdot g = F_{r2} \qquad (6.2)$$

where $F_{r2}$ is the resultant force during the closing maneuver, having the same direction as the acceleration of the mobile armature.

Throughout the stroke of the mobile armature, the useful resultant force $F_{r2}$ acts upon it, leading to a certain amount of kinetic energy stored by the mobile armature, as follows:

$$E_c = \int_{\Gamma} \mathbf{F_{r2}}\ \mathbf{dl} = \int_{d_i}^{d_f} \mathbf{F_{r2}}\ \mathbf{dl} = \int_{d_i}^{d_f} (F_{elmg,\delta} - m \cdot g)\ \mathbf{dl} \qquad (6.3)$$

where $E_c$ [J] is the kinetic energy stored by the mobile armature, Γ is the path traveled by the armature, $d_i$ and $d_f$ are the initial and final positions of the trajectory, respectively, and dl is the infinitesimal displacement element; $F_{elmg,\delta}$ is the force generated by the electromagnetic actuator, m [kg] is the mass of the moving components, and g $[m/s^2]$ is the gravitational acceleration.

The velocity of the mobile armature can be determined considering the kinetic energy expression, which also depends on the mass of the moving body:

$$E_c = \frac{m \cdot v_a^2}{2} \rightarrow v_a = \sqrt{\frac{2 \cdot E_c}{m}} \qquad (6.4)$$

where $E_c$ [J] is the kinetic energy stored in the mobile armature, and $v_a$ $[m/s]$ represents the additional velocity obtained by the mobile armature, as shown in Figure 6.1.

$$v_a = \sqrt{\frac{2}{m}} \cdot \sqrt{E_c} = \sqrt{\frac{2}{m}} \cdot \sqrt{\int_{d_i}^{d_f} (\mathbf{F_{elmg,\delta}} - m \cdot \mathbf{g})\, \mathbf{dl}} \qquad (6.5)$$

where $v_a$ [m/s] represents the additional velocity obtained by the mobile armature after covering the distance from $d_i$ to $d_f$ having accumulated the kinetic energy $E_c$, and m [kg] is its mass; the velocity characteristics of the mobile armature as a function of the traveled distance (for different magnetomotive forces generated by the excitation coil) are shown in Figure 6.2.

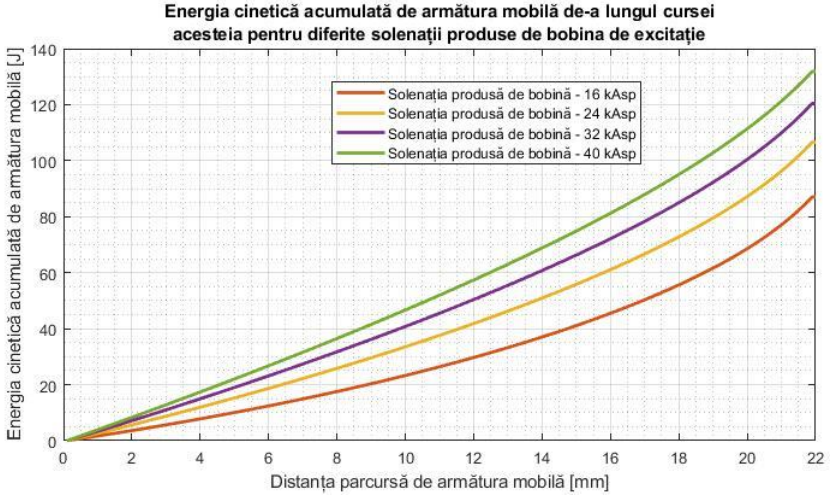


Fig. 6.1. Kinetic energy accumulated by the mobile armature during closing maneuver, depending on the distance traveled, for different magnetomotive forces generated by the excitation coil (without mechanical load)

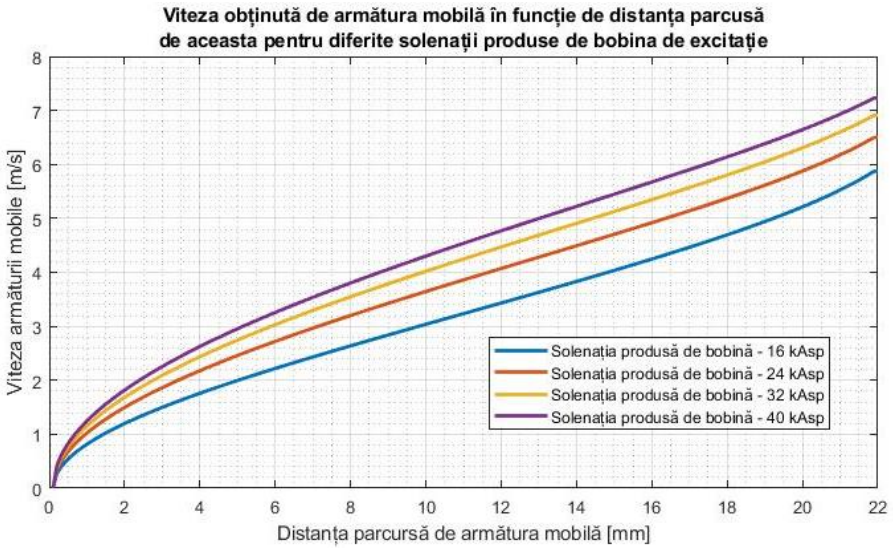


Fig. 6.2. Velocity of the mobile armature during closing maneuver, depending on the distance traveled, for different magnetomotive forces generated by the excitation coil (without mechanical load)

## 6.2. Kinematic Analysis of the Electromagnetic Actuator with Mechanical Load

The kinematic analysis of the electromagnetic actuator with mechanical load involves determining its kinetic parameters of interest, in order to evaluate the device's performance while operating as a subassembly of the mechanism in which it is integrated. Considering that the electromagnetic actuator employs a compression spring for performing the opening maneuver and to maintain the maximum air gap between the mobile and fixed armature, its influence must be determined.

### 6.2.1. Kinematic Analysis of the Electromagnetic Actuator with Mechanical Load during closing maneuver

Considering the electromagnetic actuator coupled to the mechanical load, i.e., the opening spring, the mechanical equation during the closing operation can be written as:

$$m \cdot \vec{a}_{ancl} + \vec{F}_{elmg,\delta} + \vec{F}_{res,k-\delta} + \vec{G} = 0 \rightarrow m \cdot \vec{a}_{ancl} + \vec{F}_{elmg,\delta} + \vec{F}_{res,k-\delta} + m\vec{g} = 0 \qquad (6.6)$$

where $m$ [kg] is the mass, $a_{ancl}$ $[m/s^2]$ is the acceleration, and $F_{elmg,\delta}$ [N] is the electromagnetic force developed at the air gap $\delta$; the force developed by the compression spring at a certain value of the air gap, depending on its elongation (equal to the distance traveled by the mobile armature) and on the spring constant, as well as on the precompression force is:

$$F_{res,k-\delta} = F_{res,k} + (\delta_{max} - \delta) \cdot \tau \qquad (6.7)$$

where $F_{res,k}$ [N] is the force developed by the precompressed spring, $\delta_{max}$ [m] is the maximum air gap between the fixed and mobile armature, $\delta$ [m] is the air gap at which the spring develops the force $F_{res,k-\delta}$ [N], and $\tau$ [N/m] is the spring constant.

Thus, the useful, resistant and opposing forces involved in the closing maneuver can be determined, as illustrated in the figure below:

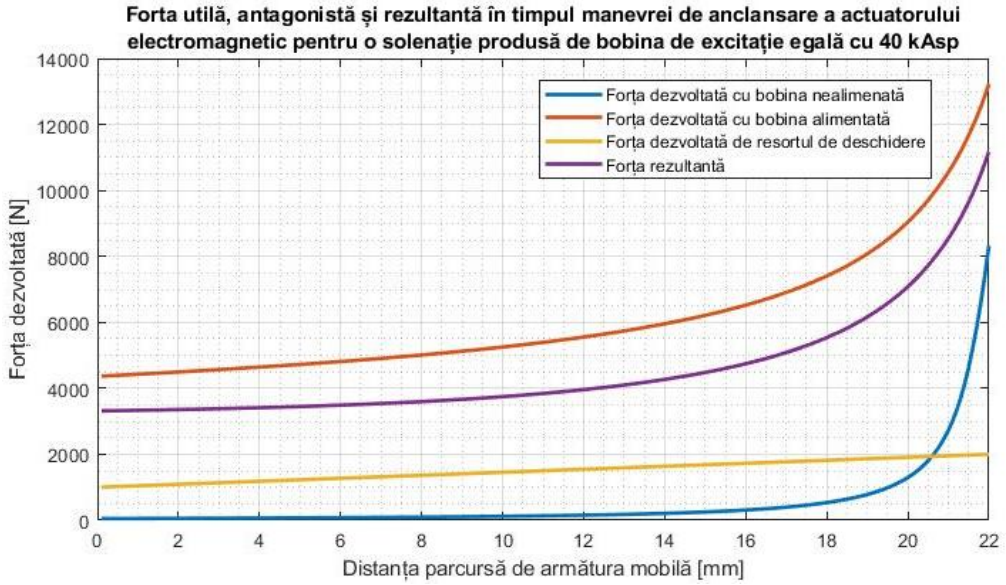


Fig. 6.3. Forces acting during the closing maneuver

Taking into account the direction of action of the forces, equation (6.6) becomes:

$$m \cdot a_{ancl} = F_{elmg,\delta} - m \cdot g - F_{res,k-\delta} = F_{r2} \qquad (6.8)$$

where $F_{r2}$ is the resultant force during closing maneuver and has the same direction as the mobile armature.

Considering all opposing forces, including the one generated by the opening spring, the resultant useful force $F_{r2}$, leads to the accumulation of kinetic energy in the mobile armature, given by:

$$E_c = \int_{\Gamma} \mathbf{F_{r2}}\ \mathbf{dl} = \int_{d_i}^{d_f} \mathbf{F_{r2}}\,\mathbf{dl} = \int_{d_i}^{d_f} (\mathbf{F_{elmg,\delta}} - m \cdot \mathbf{g} - \mathbf{F_{res,k}} - (\delta_{max} - \delta) \cdot \tau)\,\mathbf{dl} \qquad (6.9)$$

where $E_c$ [J] is the kinetic energy accumulated in the mobile armature, Γ is the trajectory along which it move, $d_i$ and $d_f$ are the initial and final points of the trajectory, and dl is the infinitesimal length of the trajectory,; $F_{elmg,\delta}$[N] is the electromagnetic force developed exerted upon the mobile armature**,** $m_a$ [kg] is the mass, and $g\ [m/s^2]$ is the gravitational acceleration.

Since the electromagnetic force and the opposing forces acting on the armature are known, the kinetic energy can be numerically integrated using the MATLAB program:

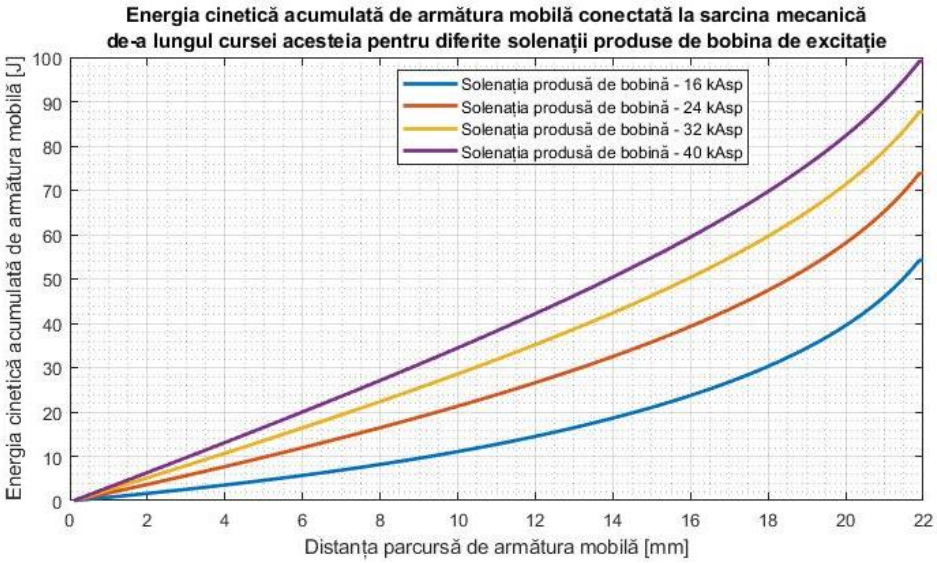


Fig. 6.4. Kinetic energy acquired by the mobile armature during closing maneuver, depending on the distance traveled, for different magnetomotive forces (with mechanical load)

Knowing the kinetic energy and the mass of the mobile armature, its velocity can be determined as:

$$v_a = \sqrt{\frac{2}{m}} \cdot \sqrt{E_c} = \sqrt{\frac{2}{m}} \cdot \sqrt{\int_{d_i}^{d_f} (\mathbf{F_{elmg,\delta}} - m \cdot \mathbf{g} - \mathbf{F_{res,k}} - (\delta_{max} - \delta) \cdot \boldsymbol{\tau})\,\mathbf{dl}} \qquad (6.10)$$

where $v_a$ [m/s] represents the additional velocity acquired by the mobile armature after it has traveled the distance between $d_i$ and $d_f$ and has accumulated the kinetic energy $E_c$[J], and m [kg] is the mass of the moving body.

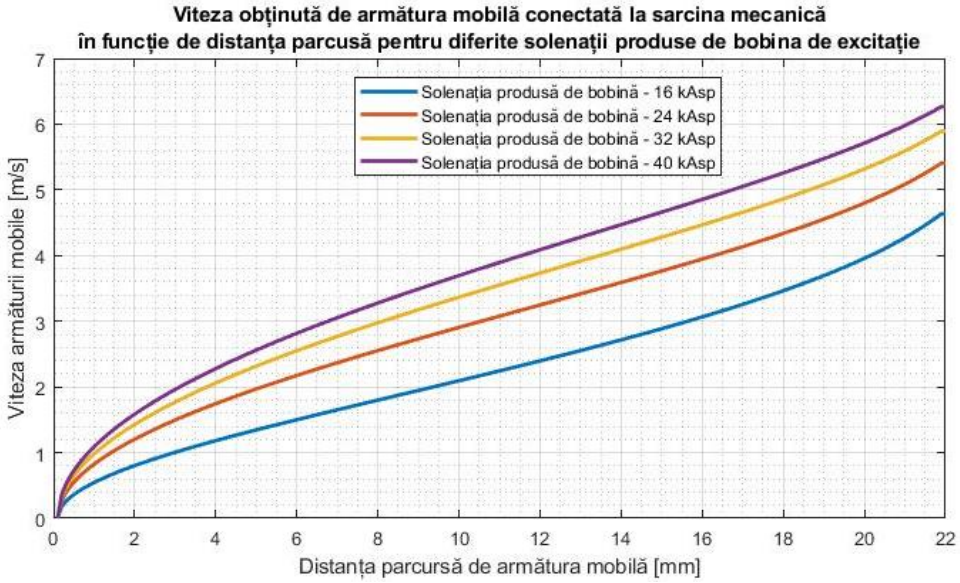


Fig. 6.5. Velocity of the mobile armature during closing maneuver, depending on the distance traveled, for different magnetomotive forces (with mechanical load)

As can be seen in the previous figure, the velocity of the mobile armature has an increasing evolution, due to the existence of a positive resultant force and, correspondingly, of an increasing kinetic energy [17].

### 6.2.2. Kinematic Analysis of the Electromagnetic Actuator with Mechanical Load During Opening Maneuver

The kinematic analysis of the electromagnetic actuator with mechanical load for the opening maneuver involves the determination of its relevant kinematic parameters, in order to establish the performance of the device in relation to the opening process, respectively to the return of the mobile armature to its initial position.

Considering the fact that the optimal magnetomotive force produced by the coil is known, when the resulting magnetic field in the electromagnetic actuator has low values in the effective air gaps, the coil can be supplied in such a way that the electromagnetic force is negligible during the maneuver.

Regarding this, the only antagonistic forces involved in the opening process of the electromagnetic actuator are the force developed by the spring and the weight of the mobile armature, as can be seen in the following equation:

$$F_{r4} = m \cdot a_{decl} = G + F_{res,k} \qquad (6.11)$$

where $F_{res,k}$ [N] is the force developed by the opening spring at the beginning of the opening maneuver, G [N] is the weight of the mobile armature, $a_{decl}$ $[m/s^2]$ is the acceleration of the mobile armature during opening maneuver, and $F_{r4}$ [N] is the resultant force during this maneuver. The three forces involved in the opening process can be observed in Figure 6.6.

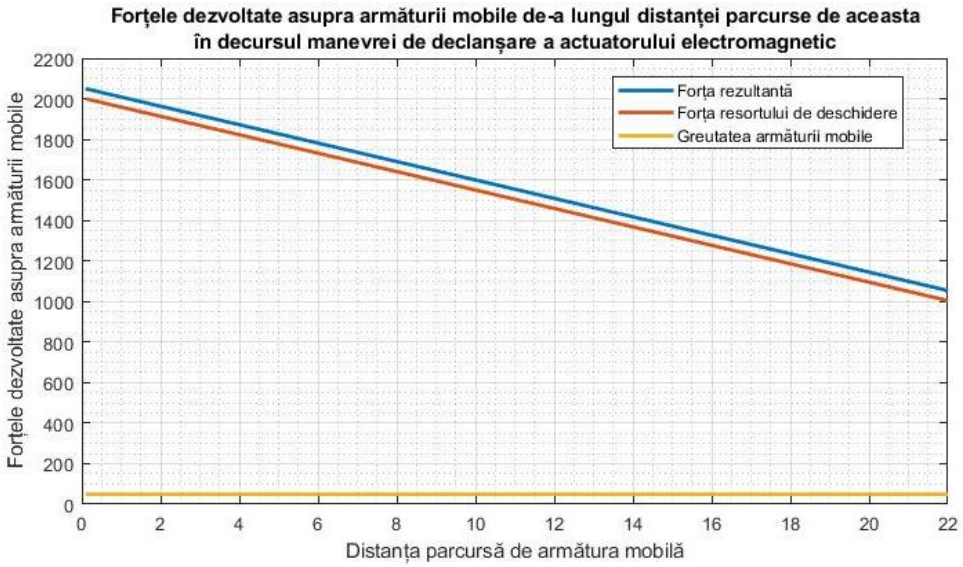


Fig. 6.6. Forces acting on the mobile armature as a function of the distance traveled by it during the opening maneuver of the electromagnetic actuator

Considering that the force acting on the mobile armature during its displacement is known, the kinetic energy stored by it can be computed according to relation 6.12, as shown in Figure 6.7.

$$E_c = \int_{\Gamma} \mathbf{F_{r4}}\ \mathbf{dl} = \int_{d_i}^{d_f} \mathbf{F_{r4}}\,\mathbf{dl} = \int_{d_i}^{d_f} (\mathbf{F_{res,k}} + \mathbf{G})\,\mathbf{dl} \qquad (6.12)$$

where $E_c$[J] is the kinetic energy accumulated by the mobile armature, Γ is the trajectory along which it moves, $d_i$ and $d_f$ are the initial and final points of the trajectory, and dl is the infinitesimal length element of this trajectory; $F_{res,k}$[N] is the force developed by the spring acting on the mobile armature, and G [N] is the weight.

The velocity of the mobile armature can be determined based on the expression of kinetic energy, which also depends on the mass of the mobile armature, as follows:

$$E_c = \frac{m \cdot v_a^2}{2} \rightarrow v_a = \sqrt{\frac{2 \cdot E_c}{m}} \quad (6.13)$$

where $E_c$ [J] is the kinetic energy accumulated by the mobile armature along the trajectory Γ, and $v_a$ [m/s] is the additional velocity obtained by the projectile as a result of the accumulation of kinetic energy $E_c$.

$$v_a = \sqrt{\frac{2}{m_a}} \cdot \sqrt{E_c} = \sqrt{\frac{2}{m_a}} \cdot \sqrt{\int_{d_i}^{d_f} (\mathbf{F_{res,k}} + \mathbf{G})\,\mathbf{dl}} \qquad (6.14)$$

where $v_a$ [m/s] represents the additional velocity obtained by the mobile armature after traveling the distance between $d_i$ and $d_f$ and accumulated the kinetic energy $E_c$[J], and m [kg] is the mass of the moving body.

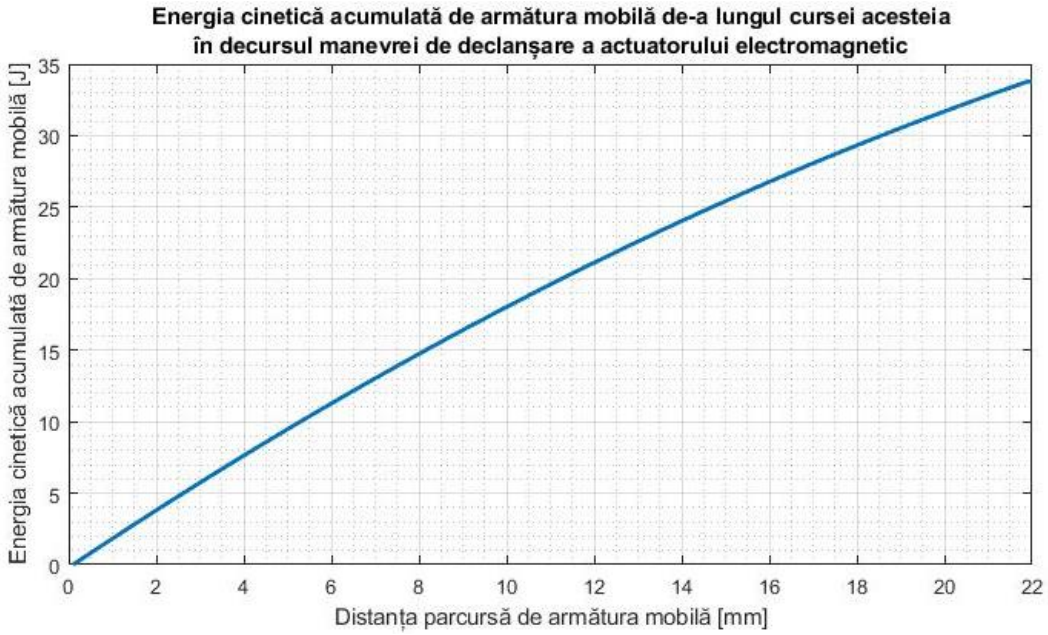


Fig. 6.7. Kinetic energy accumulated by the mobile armature as a function of the distance traveled by it during the opening maneuver of the electromagnetic actuator

Considering the above, the velocity characteristic of the mobile armature as a function of the distance traveled by it is presented in the following figure:

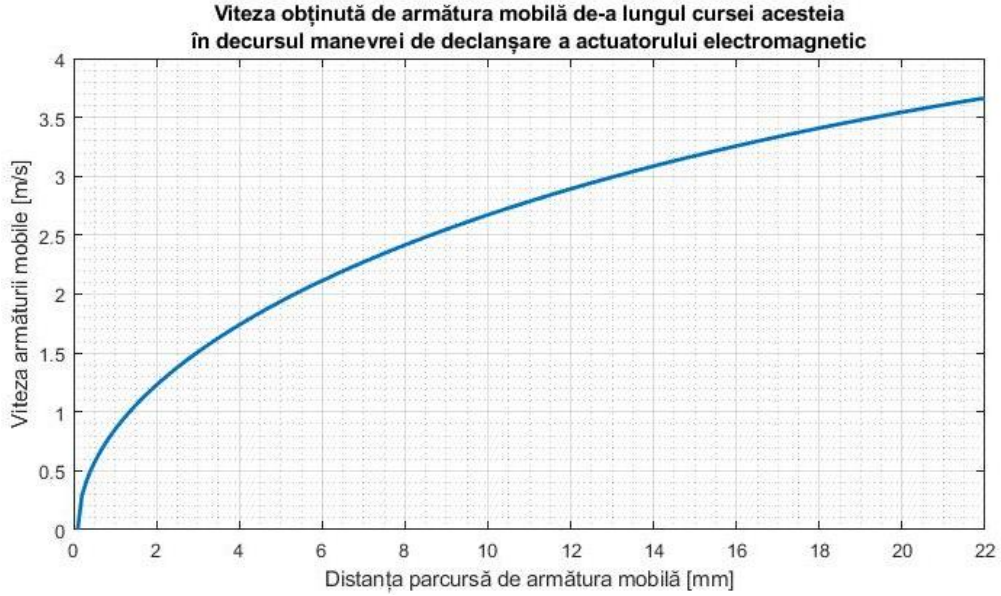


Fig. 6.8. Velocity obtained by the mobile armature as a function of the distance traveled by it during the tripping maneuver of the electromagnetic actuator

# 7. Implementation of the Experimental Model of Electromagnetic Actuator

## 7.1. General Considerations Regarding the Physical Implementation of the Experimental Model

In order to validate the analytically determined and numerically modeled solution using the FEMM software, it is necessary to implement a full-scale (1:1) experimental model, to evaluate its electrical and kinematic performance.

Obviously, in addition to the physical implementation of the main active subassemblies, namely those that generate and direct the magnetic field, the realization of auxiliary components was also required, such as spacers, internal supports, and the striker.

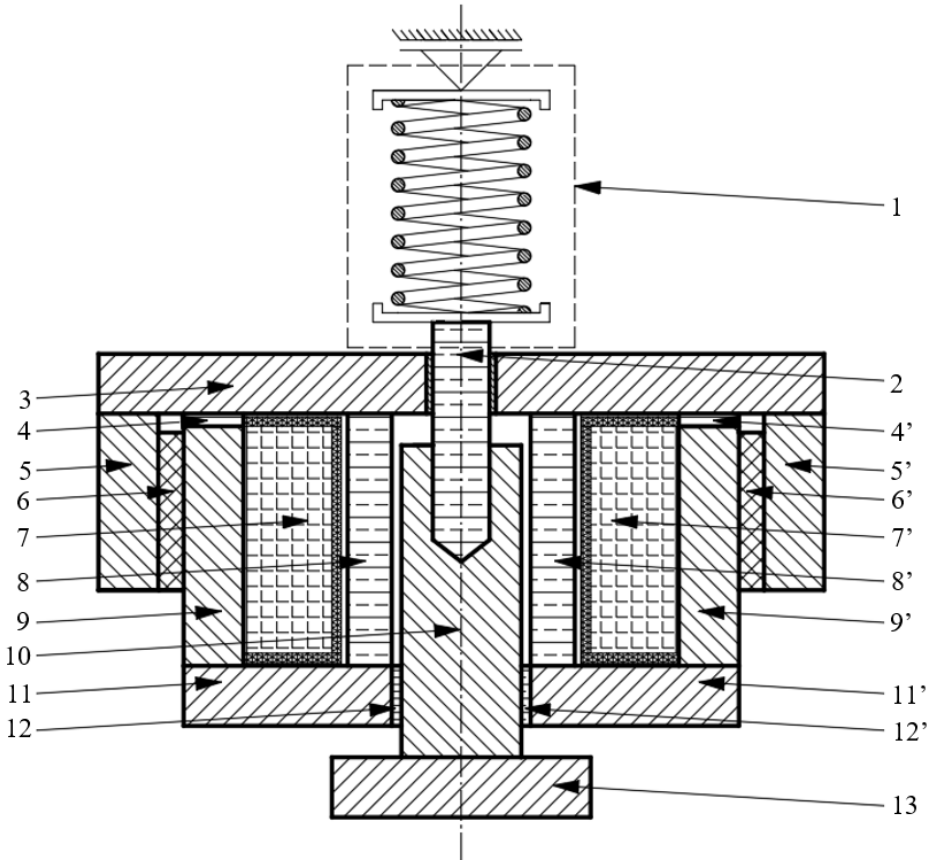


Fig. 7.1. Technical assembly drawing (in section) of the electromagnetic actuator with permanent magnets

In this regard, Figure 7.1 presents the technical assembly drawing of the electromagnetic actuator with permanent magnets, as well as its opening mechanism. According to Figure 7.1, the main subassemblies of the electromagnetic actuator with permanent magnets are as follows:

- the fixed ferromagnetic circuit**,** which is made up of the upper ferromagnetic plate (3), the two lateral ferromagnetic plates (9 and 9'), and the two lower ferromagnetic plates (11 and 11'). The lateral ferromagnetic plates (9 and 9') are separated from the upper plate (3) by two upper spacers (4 and 4') to establish the required air gap according to numerical modeling; for mechanical

reinforcement, two internal supports (8 and 8') are used, and for guiding the mobile ferromagnetic circuit, two lower spacers (12 and 12') serve as guides;

- the mobile ferromagnetic circuit**,** which consists of the striker (2), whose role is to guide the subassembly along its path, the central column (10), and the pole segment (13).
- the auxiliary ferromagnetic circuit, made up of two ferromagnetic plates (5 and 5') and two permanent magnets (6 and 6');
- the excitation coil, represented by its cross sections (7 and 7'), concentrically positioned around the central column (10), and fixed in place by the components of the fixed ferromagnetic circuit subassembly (i.e., ferromagnetic plates 3, 9, 9', 11, and 11' and supports 8 and 8').

## 7.2.Physical Implementation of the Fixed Ferromagnetic Circuit

Regarding the physical implementation of the fixed ferromagnetic circuit, Figure 7.2 shows the technical assembly drawing (in section). Considering that in Figure 7.1 the components of the electromagnetic actuator have already been labeled, the same notation is retained in the technical drawing of the fixed ferromagnetic circuit (notations indicated in parentheses):

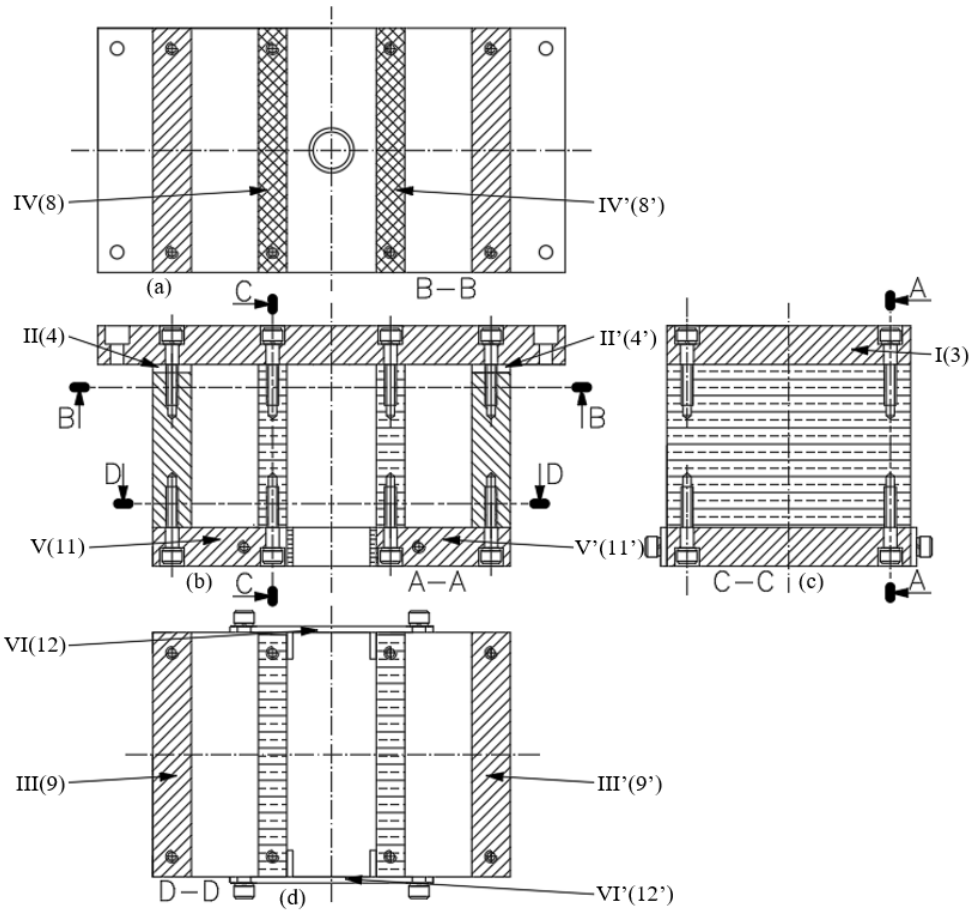


Fig. 7.2. Technical assembly drawing (in section) of the fixed ferromagnetic circuit

In Figure 7.2 (a), section B – B is shown, through the lateral ferromagnetic plates and internal supports, with a view toward the upper ferromagnetic plate. In Figure 7.2 (b), section A – A is presented, showing the entire fixed ferromagnetic circuit with the fastening holes and assembly

elements. Figure 7.2 (c) displays section C – C through the upper ferromagnetic plate, internal supports, and lower ferromagnetic plates, highlighting the fastening holes and assembly elements, and Figure 7.2 (d) presents section D – D through the lateral ferromagnetic plates and internal supports, with a view toward the lower ferromagnetic plates.

## 7.3.Physical Implementation of the Auxiliary Ferromagnetic Circuit

The auxiliary ferromagnetic circuit consists of two lateral ferromagnetic plates and two permanent magnets, whose technical drawings can be seen in the following figure:

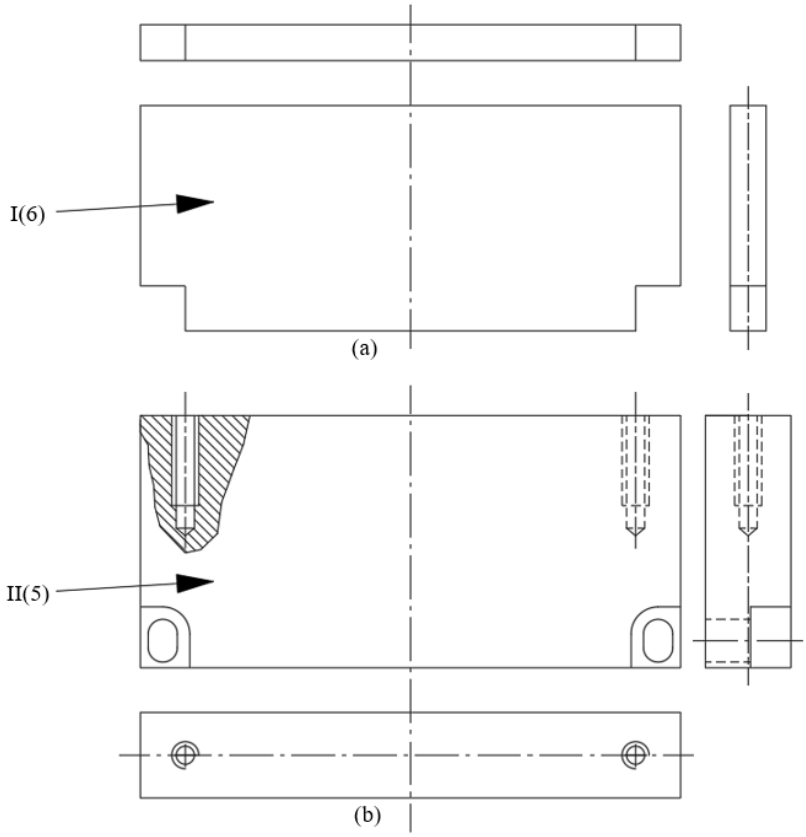


Fig. 7.3. Technical execution drawing of the permanent magnet (a) and lateral ferromagnetic plates (b) from the auxiliary ferromagnetic circuit

The auxiliary ferromagnetic circuit is composed of four components, all paired and symmetrical with respect to the assembly's axis of symmetry, namely:

- I – Permanent magnets (labeled as 6 and 6' in Figure 7.1);;
- II – Auxiliary ferromagnetic plates (labeled as 5 and 5' in Figure 7.1).

## 7.4.Physical Implementation of the Mobile Ferromagnetic Circuit

As for the physical implementation of the mobile ferromagnetic circuit, Figure 7.4 presents its technical assembly drawing (in section). Since the components of the electromagnetic actuator were already labeled in Figure 7.1, the same labeling is preserved in the drawing of the mobile ferromagnetic circuit (notations in parentheses):

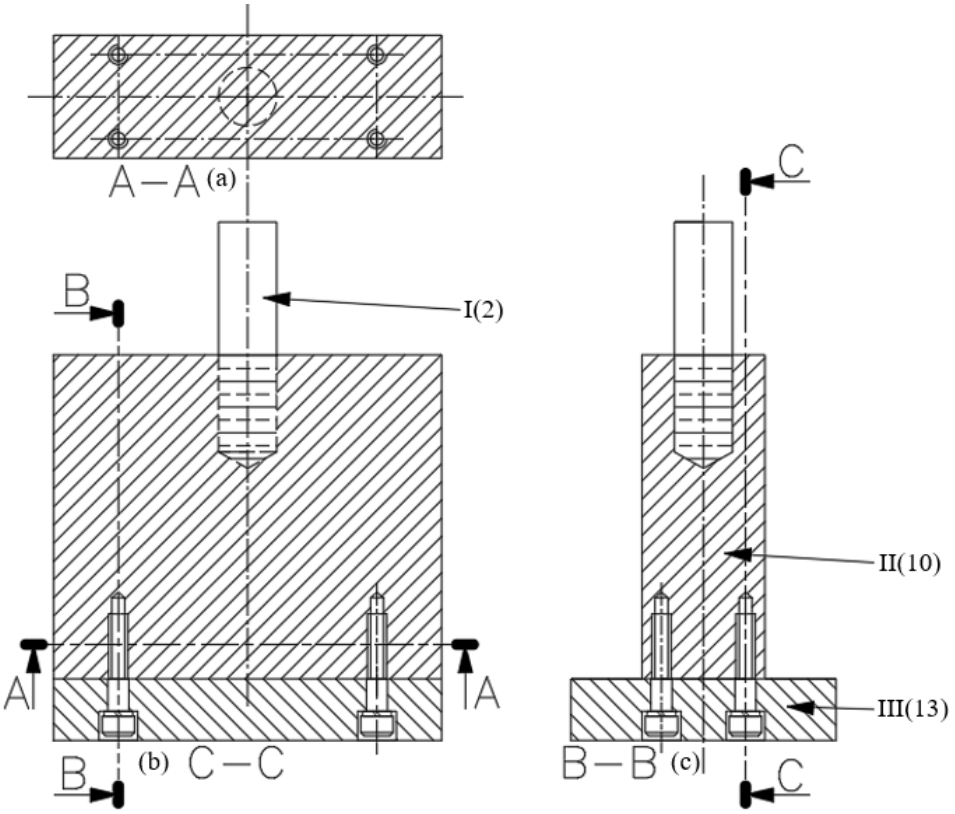


Fig. 7.4. Technical assembly drawing (in section) of the mobile ferromagnetic circuit

In Figure 7.4 (a), section A – A is shown, through the central column, with a view toward the striker (transverse section). In Figure 7.4 (b), section C – C through the central column and the pole segment is displayed, highlighting the fastening holes and assembly elements (longitudinal section). Figure 7.4 (c) presents section B – B through the central column and pole segment, also showing the fastening holes and assembly elements.

According to Figure 7.4, the mobile ferromagnetic circuit consists of three components:

- I – Striker (labeled 2 in Figure 7.1);
- II – Central column (labeled 10 in Figure 7.1);
- III – Pole segment (labeled 13 in Figure 7.1).

## 7.5. Physical Implementation of the Excitation Coil

The excitation coil consists of two distinct components: the insulating housing and the winding. Considering that the electromagnetic actuator operates at relatively low voltages and there are no significant dielectric stresses, the insulating housing is made of stratitex with a thickness of 4 mm, as shown in Figure 7.5.

The winding on the insulating housing is made from enamelled copper wire with a diameter of Φ1.5 mm ((insulated diameter Φ1.58 mm) and comprises 680 turns distributed în 17 layers and 40 turns per layer. The measured DC electrical resistance is 3.6 Ω, a value approximately equal to the computed one ($R_{calculat} = 3.53\ \Omega$).

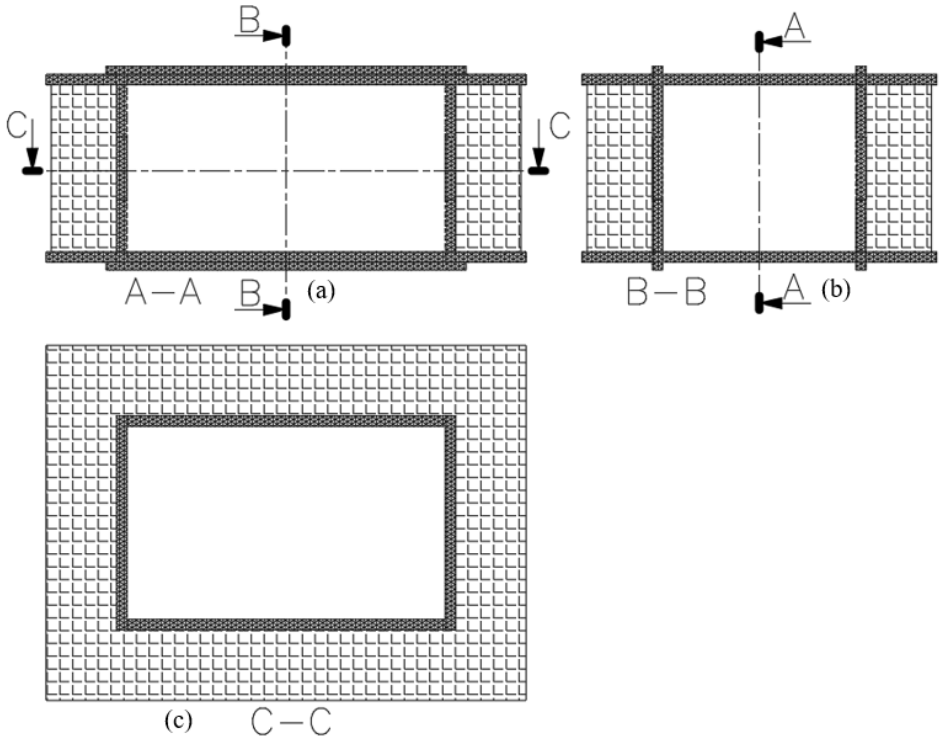


Fig. 7.5. Technical execution drawing of the excitation coil of the electromagnetic actuator

In Figure 7.5 (a), section A – A is shown (longitudinal section) through the excitation coil of the electromagnetic actuator, with a view toward its lateral area, i.e., toward the lateral ferromagnetic plates and the auxiliary ferromagnetic circuit of the actuator. Figure 7.5 (b) shows section B – B, and Figure 7.5 (c) presents section C – C, with a view toward the lower area of the coil, i.e., toward the lower ferromagnetic plates.

## 7.6.Experimental Model of the Electromagnetic Actuator with Permanent Magnets

Following the fabrication of the components presented above and their assembly using various fastening elements, the main subassemblies of the electromagnetic actuator with permanent magnets are obtained, as shown in Figure 7.6. As can be seen in Figure 7.6, the execution of all 20 components, whose technical drawings were previously presented in this chapter, results in the complete electromagnetic actuator assembly with permanent magnets, with numbering in accordance with Figure 7.1. The mobile ferromagnetic circuit (Figure 7.6 (a)) is composed of striker 2, central column 10, and pole segment 13. The fixed ferromagnetic circuit (Figure 7.6 (b)) consists of the upper ferromagnetic plate 3, upper spacers 4 and 4'.

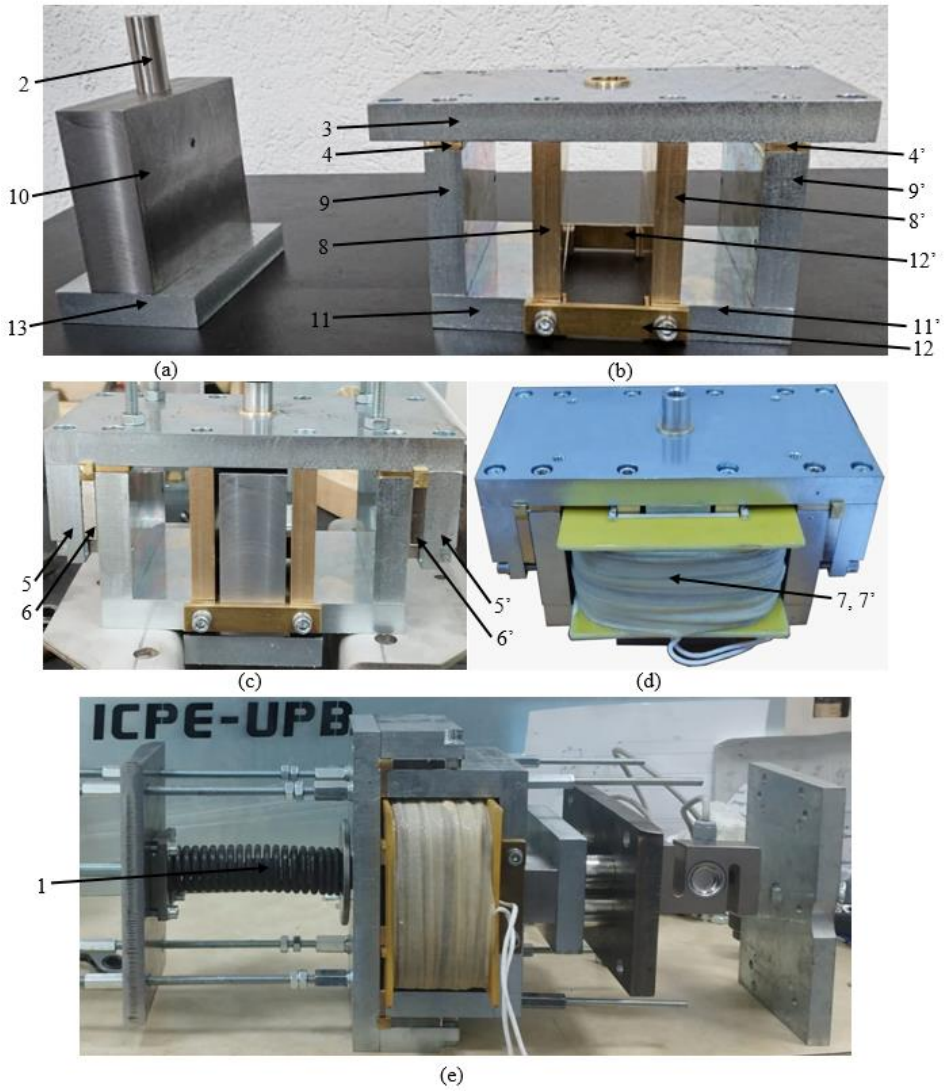


Fig. 7.6. Experimental implementation of the electromagnetic actuator model with permanent magnets; (a) – mobile ferromagnetic circuit; (b) – fixed ferromagnetic circuit; (c) – assembled ferromagnetic circuits; (d) – electromagnetic actuator assembly with permanent magnets, without opening mechanism; (e) – electromagnetic actuator assembly with permanent magnets, with opening mechanism

The auxiliary ferromagnetic circuit is shown in Figure 7.6 (c), consisting of auxiliary plates 5 and 5' and magnets 6 and 6'. These four components are mounted on the fixed circuit, into which the mobile ferromagnetic circuit is then inserted, resulting in the structure shown in Figure 7.6 (c). The excitation coil (indicated in the previous figure by 7 and 7') of the electromagnetic actuator can be seen in Figure 7.6 (d). Finally, the opening mechanism of the electromagnetic actuator (1) is shown in Figure 7.6 (e), with the spring supports mechanically attached to the striker (2) and to the fixed support (in the experimental model, a steel plate attached to the ferromagnetic circuit of the device).

# 8. Implementation of the Power Supply for the Electromagnetic Actuator with Permanent Magnets

## 8.1. General Considerations

In the performance analysis of the actuator proposed in this thesis, it is assumed that the excitation coil is supplied with a constant current (time-invariant). From a technical standpoint, the power supply would need to generate a very high voltage in order to produce a current step. However, the choice of constant current for the excitation coil allows the analytical approach developed in this work to be extended to other excitation current waveforms (under the restriction of achieving a steady-state regime). For example, in the case of constant voltage supply analysis, an iterative procedure can be employed, adjusting the excitation current until the terminal voltage is reached. This direction of research could provide opportunities for the development of new scientific works.

In order to supply the electromagnetic actuator coil with a constant current, as implemented in the numerical simulations, it would be necessary to use a high-power rectifier, fed from an alternating voltage source capable of delivering substantial power, which leads to a significantly large overall system size.

In this context, the electromagnetic actuator coil consumes a considerable amount of electrical power generated by the power source. Nevertheless, an advantage lies in the fact that the energy source must be capable of delivering this power for only a short period of time (during the switching operation), namely while the mobile armature transitions from the lower resting position to the upper resting position.

Considering the aforementioned aspects, a high-power energy source was implemented using an electrolytic capacitor bank [18], whose operating principle is described in the following subsections.

## 8.2. Justification for Choosing the Energy Source for the Electromagnetic Actuator

To meet the required performance, the electromagnetic actuator must be equipped with an appropriate power supply. The choice of a capacitor bank as the optimal technological solution offers the following advantages:

- the energy source composed of electrolytic capacitors can be charged from any alternating voltage source, regardless of its power, since it includes an autotransformer as well as charging current limiting resistors;
- the amplitude of the current through the electromagnetic actuator excitation coil can be easily adjusted by varying the capacitor bank's charging voltage; in turn, the voltage at the capacitor bank terminals is limited only by the number of capacitors connected in series.

## 8.3. Main Components of the Electromagnetic Actuator Power Supply

To study the dynamic behavior of the electromagnetic actuator, an experimental model of the power supply was implemented, which includes 16 capacitors. These 16 capacitors are grouped into 4 modules, with each module consisting of 4 capacitors connected in parallel, as shown in the figure below::

Fig. 8.1. Capacitor modules of the power supply for the electromagnetic actuator with permanent magnets

Each capacitor in the energy source has a capacitance of $C_{ind} = 8200\ \mu F$, and a maximum charging voltage of 450 Vcc. As previously mentioned, each module contains 4 capacitors in parallel, and the entire energy source consists of 4 such modules.

As mentioned earlier, the energy source can be charged from an alternating voltage source. Given that the most common AC voltage for single-phase low-voltage electrical installations is 230 V AC, the power supply was designed to operate from this voltage level, according to the circuit diagram in Figure 8.2.

The electrical diagram of the power supply includes an auxiliary circuit for the controlled charging and discharging of each capacitor module, and contains the following elements:

- the main circuit breaker $Q_{gen}$;
- autotransformer ATR (230 V/ 0...250 V);
- local circuit breakers $Q_1$, $Q_2$, $Q_3$, $Q_4$;
- transformers $T_1$, $T_2$, $T_3$, $T_4$ (220 V / 285 V);
- single-phase rectifier bridges PR1, PR2, PR3, PR4;
- charging current limiting resistors $R_{L1}$, $R_{L2}$, $R_{L3}$, $R_{L4}$;
- discharging resistors $R_{D1}$, $R_{D2}$, $R_{D3}$, $R_{D4}$;
- polarized capacitor modules $M_1$, $M_2$, $M_3$, $M_4$;
- freewheeling diodes DRL1, DRL2, DRL3, DRL4 [19];
- contactor $K_1$;
- discharging circuit breakers $Q_{d1}$, $Q_{d2}$, $Q_{d3}$, $Q_{d4}$;
- circuit breaker $Q_K$.

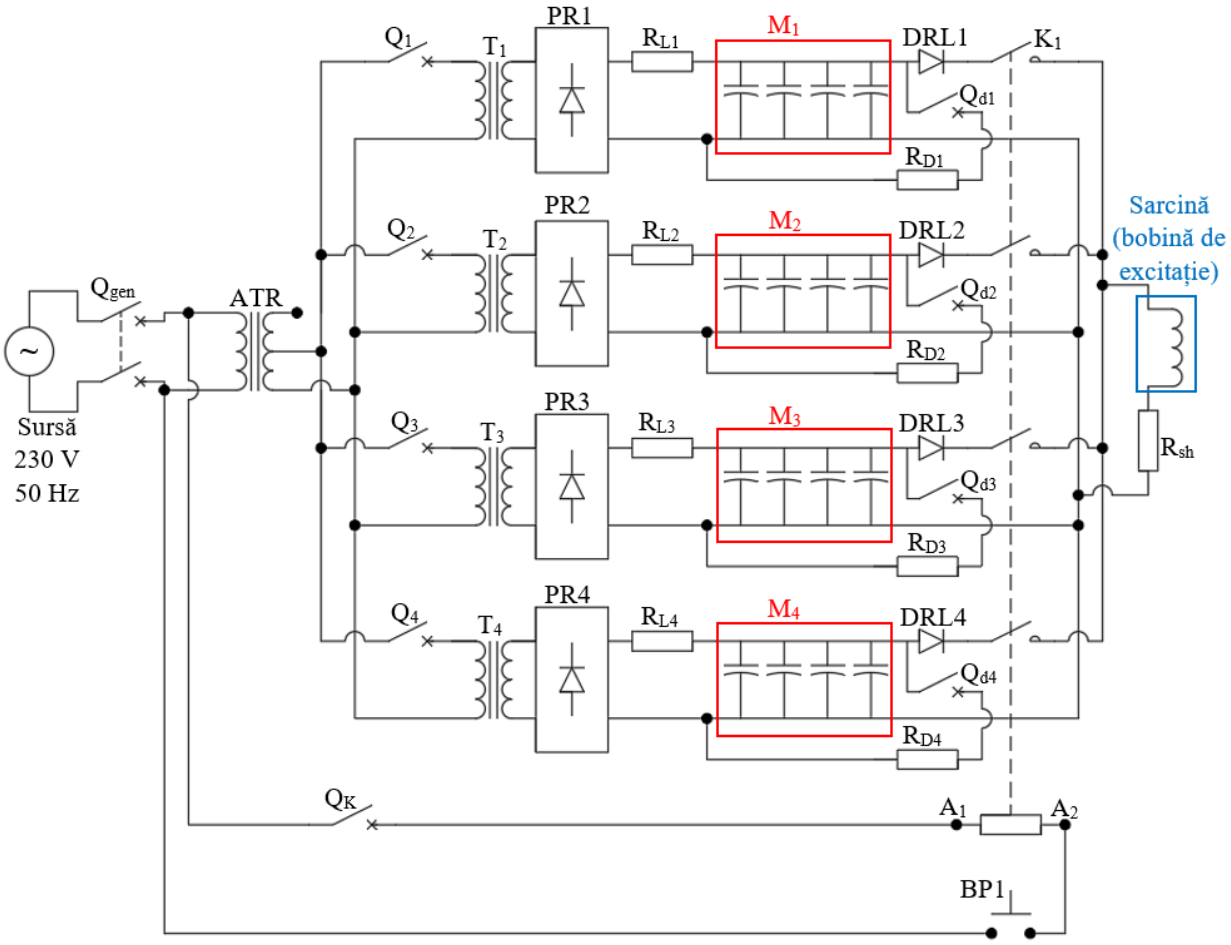


Fig. 8.2. Simplified electrical diagram of the power supply for the electromagnetic actuator

## 8.4. Operating Principle of the Electromagnetic Actuator Power Supply

### 8.4.1. Charging the Capacitor Bank

To charge the capacitor modules, the main circuit breaker $Q_{gen}$, is closed, the desired output voltage is set on the autotransformer ATR, and the local circuit breakers $Q_1, Q_2, Q_3, Q_4$, are closed in sequence as needed, while the other switching devices remain open.

During capacitor charging, the voltage equation can be written as:

$$u_c(t) = U_C\left(1 - e^{-\frac{t}{T_1}}\right) \quad (8.1)$$

where $T_1[s]$ is the time constant of the charging circuit.

### 8.4.2. Discharging the Capacitors on the Auxiliary Circuit's Discharge Resistor

To discharge the capacitors through the auxiliary circuit resistors ($R_{D1}$ ... $R_{D4}$), the circuit breakers ($Q_{d1}$ ... $Q_{d4}$), are closed, while the other switching devices remain open. The discharge resistors in the auxiliary circuits were implemented to prevent accidents, and the capacitor modules may remain connected to the discharge resistors while not in use.

During capacitor discharge through a resistor, the voltage equation can be written as:

$$u_C(t) = U_C \cdot e^{-\frac{t}{T_2}} \quad (8.2)$$

where $U_C[V]$ is the capacitor terminal voltage before discharge, and $T_2[s]$ is the time constant of the discharge process.

### 8.4.3. Discharging the Capacitors into the Electromagnetic Actuator Excitation Coil

The discharge of the capacitor modules into the electromagnetic actuator excitation coil is influenced by certain kinetic and electromagnetic phenomena that occur during the actuator's operation, specifically during the closing and opening maneuvers.

As the air gap decreases, magnetic circuit saturation occurs (since the magnetomotive force produced by the coil becomes very high), causing the actuator to operate along the B – H curve in a region with reduced relative magnetic permeability. Based on the above, it can be stated that the inductance of the coil is a time-dependent function, which depends both on the position of the mobile ferromagnetic circuit along its stroke and on the current flowing through the winding:

$$L_b(t) = f\big(s(t), i(t)\big) \quad (8.3)$$

where $L_b(t)$ is the inductance at time t, $s(t)$ is the position of the mobile ferromagnetic circuit relative to the fixed part, and $i(t)$ is the instantaneous coil current.

The voltage equation corresponding to the discharge of the capacitor module into the excitation coil of the electromagnetic actuator can be written as:

$$u_c(t) + u_R(t) + u_L(t) = 0 \quad (8.4)$$

where $u_R(t)$ is the voltage drop across the coil resistance, and $u_L(t)$ is the voltage associated with its inductance. Considering the expression for the current through the capacitors and the fact that it is equal in all circuit elements, results in:

$$i_R(t) = i_L(t) = i_C(t) = C \cdot \frac{du_c(t)}{dt} \quad (8.5)\ [20]$$

This yields the expression of the differential equation describing the capacitor module voltage during its discharge into the excitation coil of the electromagnetic actuator:

$$L\big(s(t), i(t)\big) \cdot C \cdot \frac{d^2u_c(t)}{dt^2} + RC \cdot \frac{du_c(t)}{dt} + u_c(t) = 0 \quad (8.6)$$

where $u_c(t)$ is the voltage at the capacitor module terminals, $C$ is the capacitance, $R$ is the coil resistance (measured in DC), and $L$ is the inductance, which depends on the position $s(t)$ of the mobile ferromagnetic circuit and the current t, and $i(t)$ at time t.

# 9. General Considerations Regarding Research Conducted with the Experimental Model of the Electromagnetic Actuator

## 9.1. General Considerations Regarding Research Conducted with the Experimental Model of Electromagnetic Actuator

In order to quantify the performance of the experimental model of the electromagnetic actuator and to compare it with the numerical one, various measurements must be performed to determine different electromagnetic and kinetic parameters of the actuator.

## 9.2. Measurement of the Magnetic Flux Density in the Air Gap of the Electromagnetic Actuator

To compare the experimental model with the numerical model of the electromagnetic actuator, respectively to validate the magnetic field solution, the magnetic flux density in the main air gap of the electromagnetic actuator was measured when it was not powered. In this case, the magnetic field is produced strictly by the permanent magnets, and the magnetic flux density was measured at an accessible point in the main air gap, as shown in the following figure:

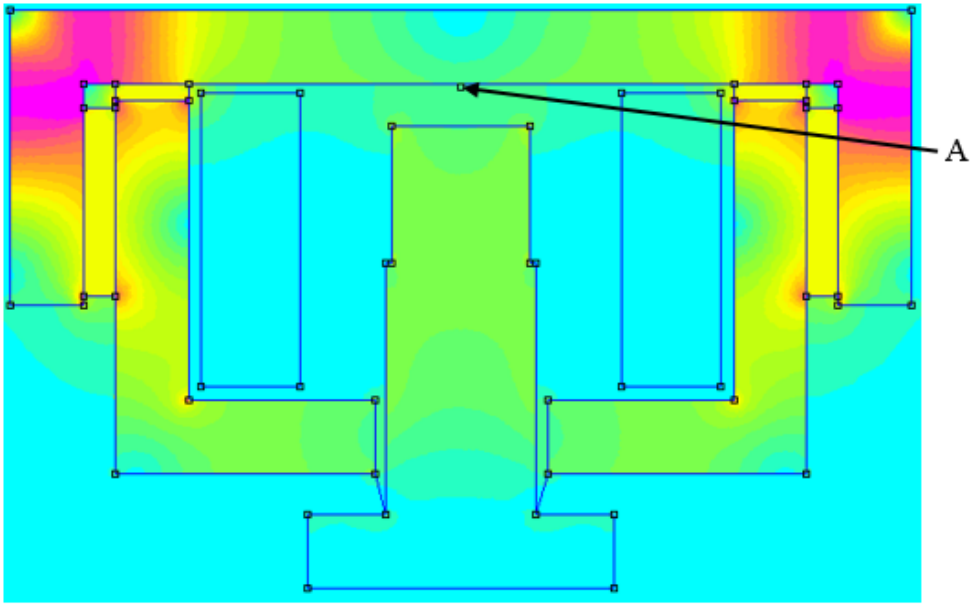


Fig. 9.1. Experimental measurement of the magnetic flux density in the main air gap of the electromagnetic actuator

According to the previous figure (9.1), the experimental measurement of the magnetic flux density was performed by positioning the Gaussmeter probe at point A.

Regarding the experimental measurement of the magnetic flux density, the measured values are presented in Figure 9.2, and in order to compare the performances of the experimental model with the numerical one, the magnetic flux density values computed using the FEMM software were also included. From the analysis of Figure 9.2, it can be observed that the relative errors are smaller for reduced air gaps, and as the air gap increases, the relative errors also increase.

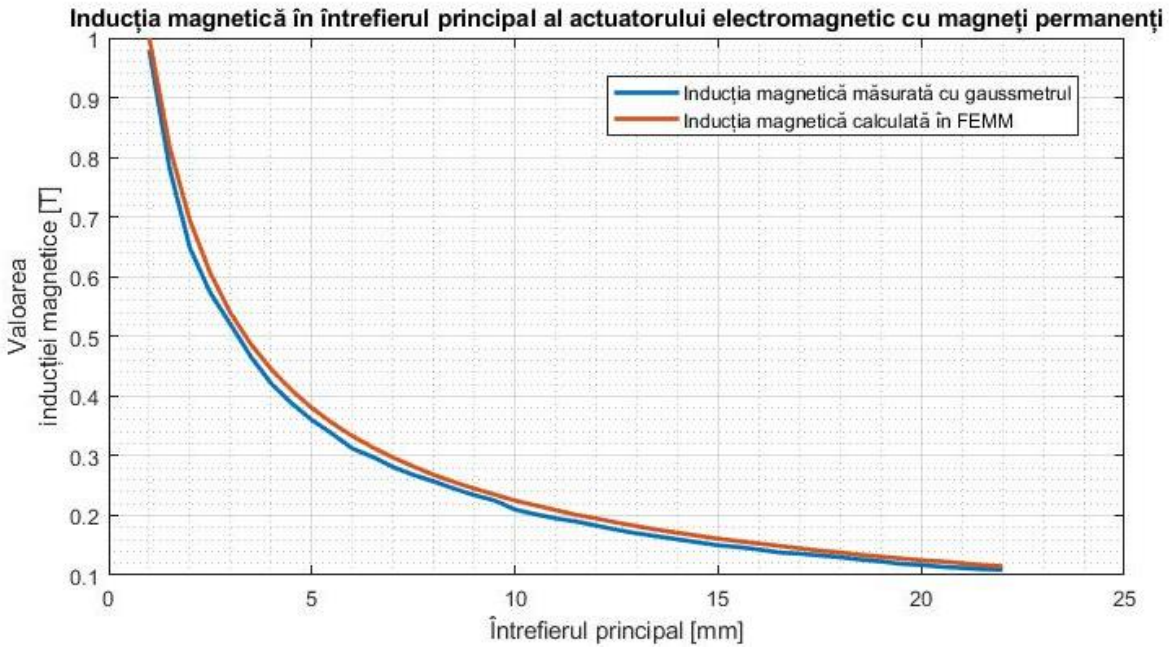


Fig. 9.2. Measured and computed magnetic flux density in the main air gap

## 9.3. Oscillographic Recording of the Waveform of the Electric Current through the Coil and the Displacement of the Mobile Ferromagnetic Circuit

### 9.3.1. General Considerations Regarding the Experimental Setup

To experimentally study the operation of the electromagnetic actuator with permanent magnets during closing and opening maneuvers, it was powered using the energy source designed and presented in Chapter 8.

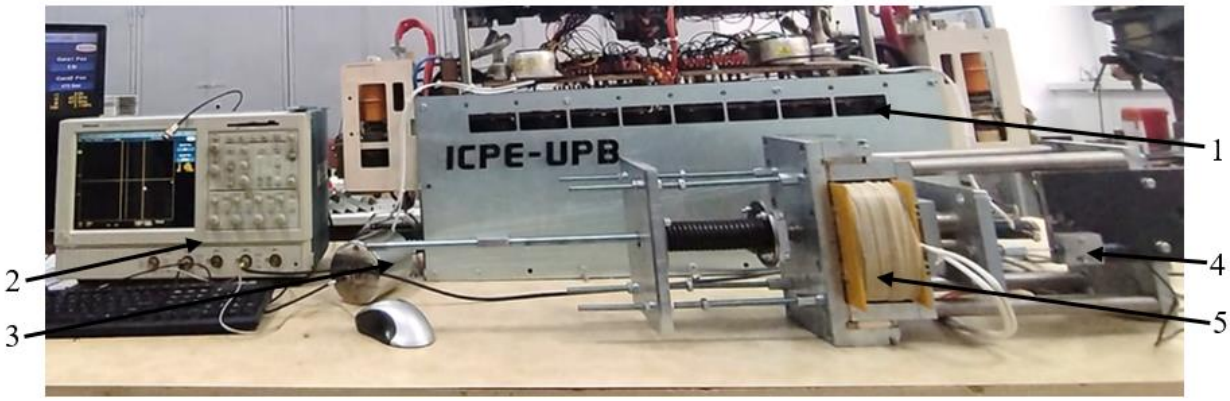


Fig. 9.3. Experimental setup for the oscillographic recording of the waveform of the electric current absorbed by the excitation coil of the electromagnetic actuator and the displacement of the mobile ferromagnetic circuit during closing and opening maneuvers

As can be seen in the previous figure, the main components of the setup are: the energy source (1), the oscilloscope (2) which receives the voltage from the coaxial shunt terminals (3) and

from the displacement transducer (4), and obviously the experimental model of the electromagnetic actuator with permanent magnets (5).

### 9.3.2. Oscillographic Recording of the Electric Current Waveform through the Coil and the Displacement of the Mobile Ferromagnetic Circuit during the Closing Maneuver of the Electromagnetic Actuator

To study the operation of the electromagnetic actuator during the closing maneuver, the capacitor modules were charged at different voltages, and the electric current and displacement were acquired after powering, as shown in Figure 9.4:

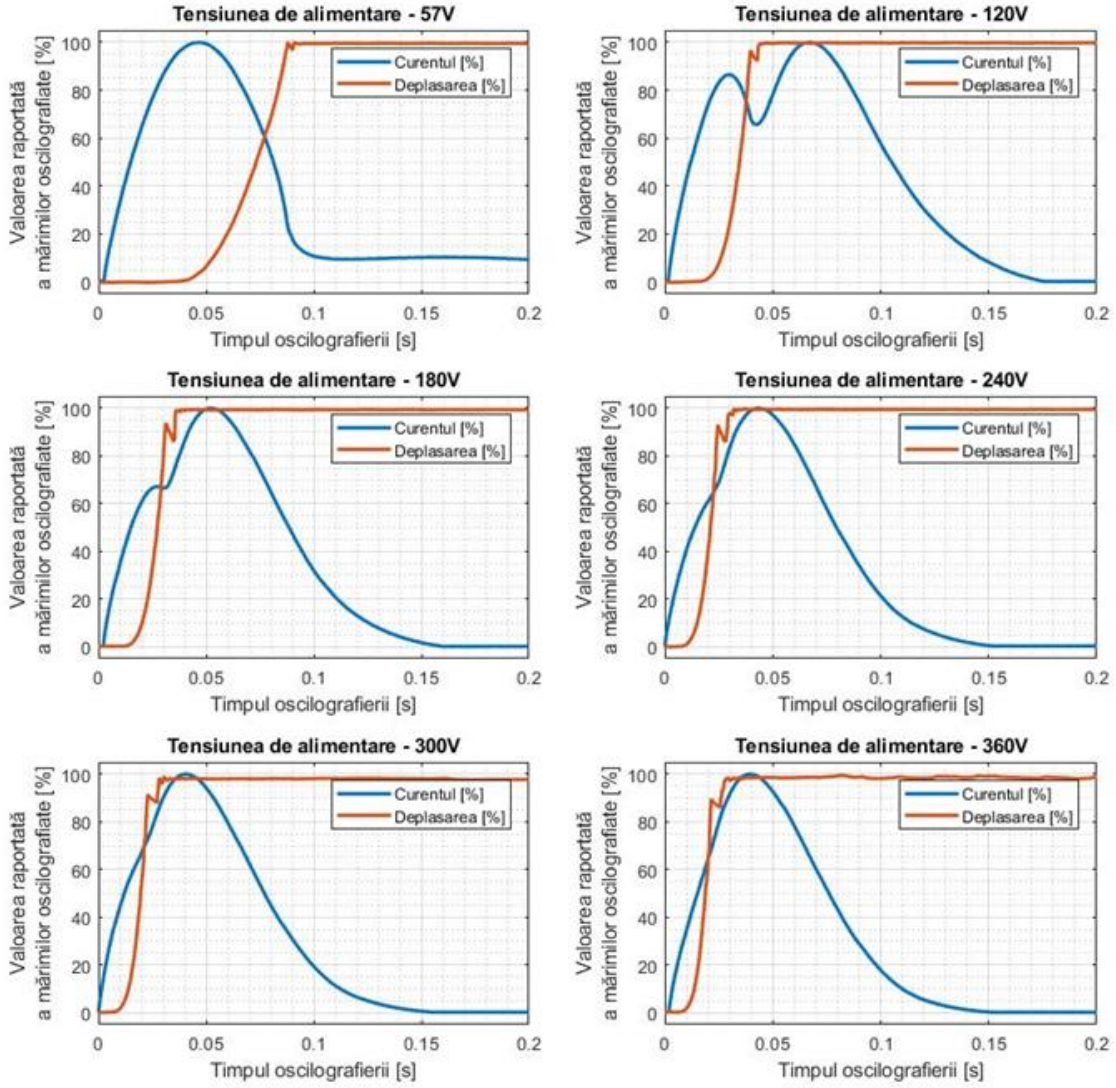


Fig. 9.4. Oscillographic recording of the absorbed current by the excitation coil and the displacement of the mobile ferromagnetic circuit on the same oscilloscope time base, during the closing maneuver, for different charging voltages of the energy source

To display on the same graph both the waveform of the electric current and the displacement characteristic of the mobile ferromagnetic circuit as a function of time, the use of relative quantities

was adopted. Thus, displacement starts at 0% (maximum air gap) and ends at 100% (minimum air gap), and the electric current value is reported relative to its maximum value (the maximum current value obtained in the aperiodic regime corresponding to 100%).

The discharge of the electric capacitors during the opening maneuver of the electromagnetic actuator leads to an aperiodic regime, according to Figure 9.4.

### 9.3.3. Oscillographic Recording of the Electric Current Waveform through the Coil and the Displacement of the Mobile Ferromagnetic Circuit during Opening Maneuver of the Electromagnetic Actuator

To study the operation of the electromagnetic actuator during the opening maneuver, the capacitor modules were charged at different voltages (similar to the works [21], [22]), and the electric current and displacement were acquired after powering, as shown in Figure 9.5.

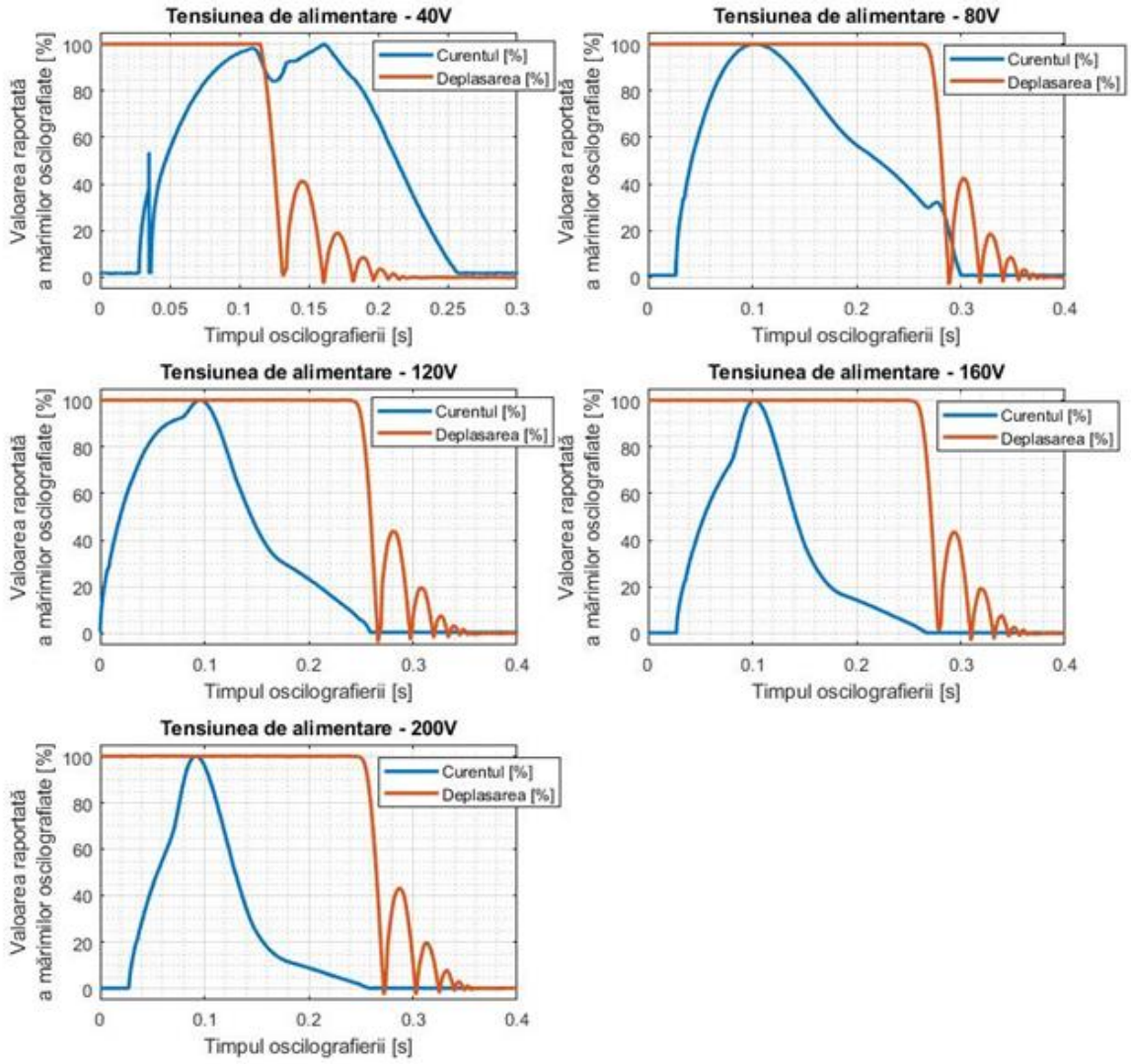


Fig. 9.5. Oscillographic recording of the absorbed current by the excitation coil and the displacement of the mobile ferromagnetic circuit on the same oscilloscope time base, during the opening maneuver, for different charging voltages of the energy source

Similar to the characteristics presented in Figure 9.4, in Figure 9.5 the use of relative quantities was adopted to display on the same graph both the waveform of the electric current and the displacement characteristic of the mobile ferromagnetic circuit as a function of time. Thus, displacement starts at 100% (minimum air gap) and ends at 0% (maximum air gap), and the electric current value is reported relative to its maximum value (the maximum current value obtained in the aperiodic regime corresponding to 100%).

## 9.4. Measurement of the Force Exerted on the Mobile Ferromagnetic Circuit

The measurement of the force exerted on the mobile ferromagnetic circuit was performed for different air gaps, using a piezoelectric force transducer, without powering the excitation coil of the electromagnetic actuator. Thus, the force developed by the electromagnetic actuator with permanent magnets along the path of its mobile armature was determined, the measurement step being 0.5 mm (from 1 mm to 22 mm). For performing the measurements, an intermediate component was mounted on the pole segment of the electromagnetic actuator, to which the force transducer was mechanically fixed, as shown in Figure 9.6.

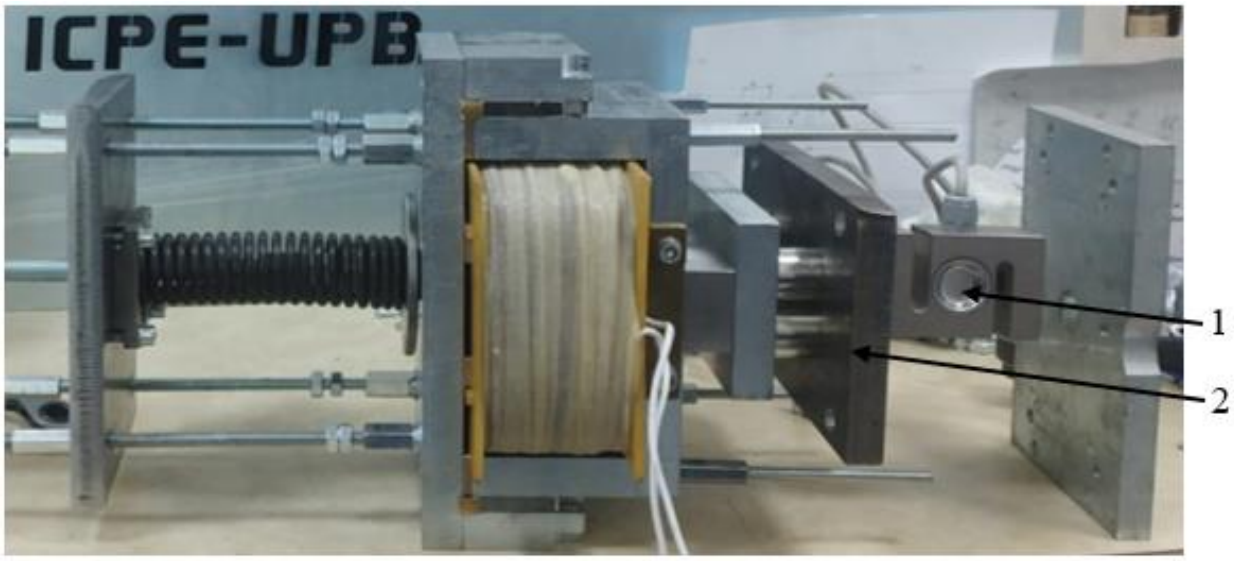


Fig. 9.6. Main components used for the experimental determination of the force exerted by the electromagnetic actuator with permanent magnets: (1) – piezoelectric force transducer; (2) – intermediate component

Thus, the experimental results obtained are compared with those computed numerically, as shown in Figure 9.7. Unlike the magnetic flux density measurements (where the computed value was always higher than the measured one for the same air gap), in the case of force, the experimentally determined values can be either lower or higher than the numerically computed ones.

According to Figure 9.7, at reduced air gap values, the error between the computed and measured force is relatively small. Small relative errors are obtained at reduced air gaps (similar to the magnetic flux density measurements) because the end effect in the air gap region has less influence.

As can be observed, high relative errors (generally between 5% and 7%) occur for high-value air gaps (greater than 11 mm), where the force value is relatively low. Considering that the force can vary by two orders of magnitude along the path of the mobile ferromagnetic circuit, combined with the numerical results obtained at reduced air gaps, it was necessary to choose a transducer whose maximum admissible force is 10 kN (approximately one ton-force). The disadvantage of choosing a transducer with a high maximum measured force is its reduced sensitivity, i.e. a resolution of 5 N, which can induce certain measurement errors (especially for high air gaps – greater than 11 mm, where the measured force is less than or equal to 100 N).

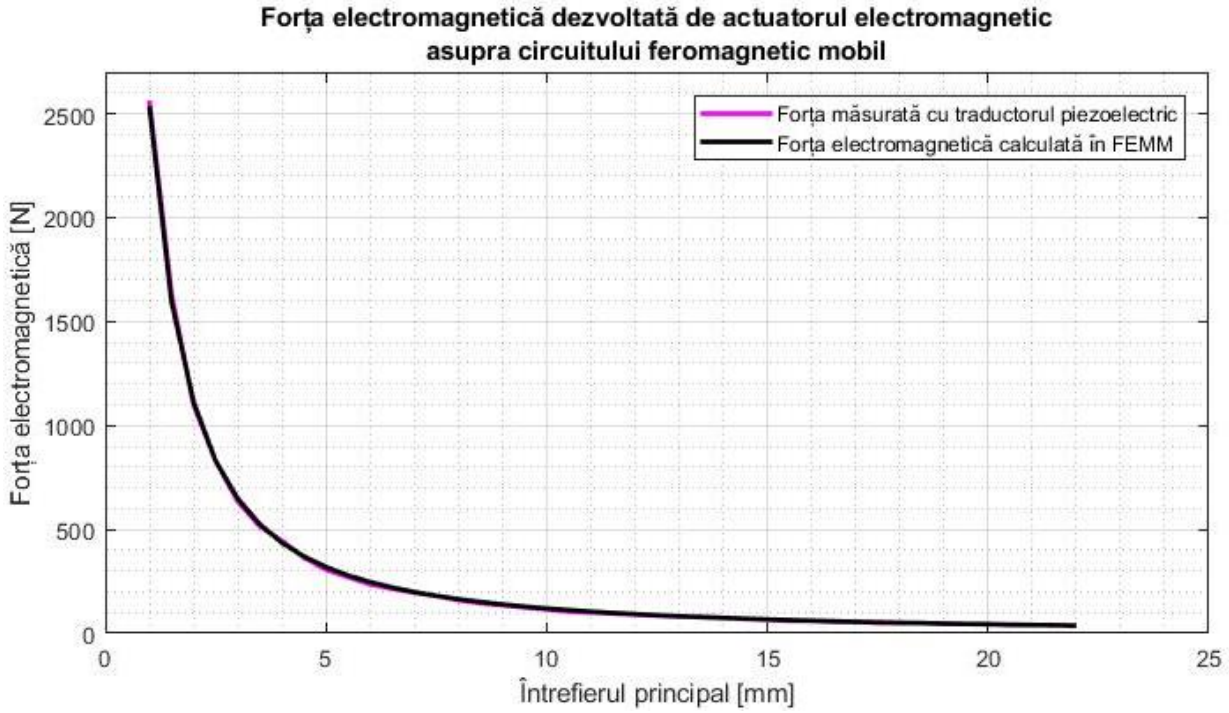


Fig. 9.7. Measured and computed electromagnetic force as a function of the air gap

Even though for high air gaps and low forces the transducer leads to force measurements with errors up to 5% ... 6%, the measured values are very close to the computed ones, which indicates the correctness of the numerical electromagnetic field model of the actuator with permanent magnets.

## 10. Conclusions

The present doctoral thesis aims to develop a new electromagnetic actuator with permanent magnets that achieves superior performance compared to existing solutions. In this context, Chapter 2 provided an overview of the current State of the Art of electromagnetic actuators with permanent magnets, as well as the main solutions commonly encountered in technical applications. Five existing structural solutions were presented, featuring both planar-parallel and axisymmetric geometries. Although the operating principle and the main parts are generally similar across these solutions, the geometrical differences among them can lead to significantly different performances.

Thus, the novelty of this doctoral thesis consists in development of a new model of electromagnetic actuator with permanent magnets, featuring an optimized geometry, detailed in Chapter 3. The key geometric improvement lies in the presence and optimal sizing of the pole segment, as well as in the optimal positioning of the auxiliary ferromagnetic circuit relative to the other parts of the actuator.

Starting from the advantages and disadvantages highlighted in the current State of the Art, the thesis presents the operating principle of the electromagnetic actuator with permanent magnets, both from the kinematic and the electromagnetic field perspectives, as detailed in Chapter 3.

For the four operating states of the actuator—maximum air gap resting position, closing maneuver, minimum air gap resting position, and opening maneuver - the actuator's behavior was described from both electromagnetic and kinematic viewpoints.

Furthermore, the main parts of the actuator were dimensioned, as outlined in Chapter 4, so that the mass and volume of the actuator are minimized to improve material efficiency and spatial integration within the larger mechanism. The main components of the actuator were dimensioned accordingly, and the primary electric and magnetic parameters which describe the operation principle were also determined.

Considering that the actuator’s mechanical performance depends on its electromagnetic parameters, it was necessary to conduct a numerical modeling of the electromagnetic actuator with permanent magnets, as presented in Chapter 5. The magnetic field was simulated in all four operating states of the actuator, focusing on how electric and magnetic parameters influence the achievement of optimal mechanical parameters. The original scientific contributions of this chapter include the analysis of actuator operation under various magnetomotive forces produced by the excitation coil, and the main mechanical parameterst were computed and discussed in Chapter 6. Unlike other scientific papers in which the electromagnetic actuator is modeled for a single magnetomotive force, in this thesis a wider range of magnetomotive forces are implemented, to study the influence of this parameter (and, by extension, the coil current) on mechanical parameters such as: the force developed by the actuator, the acceleration and velocity obtained by the mobile ferromagnetic circuit, and its accumulated kinetic energy.

Knowing these parameters allowed for the determination of the operating state and the establishment of all dependencies between the variables as functions of time or displacement, for both the closing and opening maneuvers.

Moreover, the kinematic behavior was studied under no-load operation and under the influence of a mechanical load, represented by the opening spring.

To validate the numerical results, the physical implementation of the electromagnetic actuator with permanent magnets was realised and presented in Chapter 7. Therefore, Chapter 7 presents the technical drawings of the actuator's main subassemblies, necessary for manufacturing the individual components. This chapter also details the materials used and the manufacturing technologies and processes applied. A key aspect lies in the assembly of all components to realize the actuator, with technical drawings provided for the fastening elements and connections.

In order to operate the actuator, it was necessary to design and implement a dedicated power supply, consisting of electrolytic capacitor banks and auxiliary charging/discharging circuits, thoroughly presented in Chapter 8. This chapter explains the choosing of such a power source and describes its main components. The operating principle of the energy source is structured in three subchapters that address the charging of the capacitors, their discharge on the excitation coil, and discharge on the auxiliary resistor.

One of the most important parts of the thesis is Chapter 9, which presents in detail the behavior of the experimental model of electromagnetic actuator with permanent magnets. Magnetic flux density in the actuator's air gap was measured and compared to the numerically determined values. Additionally, the force exerted on the mobile ferromagnetic circuit was measured and compared to values obtained through finite element analysis (in FEMM). In both sets of measurements, the relative errors were small (generally in the range of 1% to 5%), primarily caused by edge effects due to the 2D planar-parallel geometry. These results confirm the accuracy of the numerical model and the optimal performance of the experimental actuator.

All subassemblies were designed, optimized, and correlated to ensure the intended functionality, since the mechanical and electrical performance of the actuator with permanent magnets depends on each of its components.

## 11.References

[1] – C – H. Lee, B.H. Shin, Y-B Bang, "Designing a Permanent – Magnetic Actuator for Vacuum Circuit Breakers Using the Taguchi Method and Dynamic Characteristic Analysis", IEEE Transactions on Industrial Electronics, Vol. 63, No. 3, 2016, pp. 1655 – 1664.
[2] – P. Immonen, V. Ruuskanen, J. Pyrhönen, "Moving magnet linear actuator with self – holding functionability", IET Electrical Systems in Transportation,Vol. 8, No. 3, 2018, pp. 182 – 187.
[3] – S.J. Kim, J.H. Hur, Y.I. Kim C.M. Yun, "One – Coil Long – Stroke Permanent Magnetic Actuator Design Applied to Load Breaker Switch for Railway", MDPI Applied Sciences, Vol. 12, No. 16, 2022.
[4] – E.Choi, J.Ma, "Development of Permanent Magnetic Actuator for a solid insulated vacuum circuit breaker", International Conference on Electric Power Equipment – Switching Technology, 1 oct. 2015, pp 462 – 465.
[5] – J.Jiang, H.Lin, S.Fang, "Multi-Objective Optimization of a Permanent Magnet Actuator for High Voltage Vacuum Circuit Breaker Based on Adaptive Surrogate Modeling Technique", Energies, MDPI, Vol 12, No. 24, dec. 2019.
[6] – A. Radulian, M. Maricaru, I.V. Nemoianu, R. Crețu, "New solution of linear DC actuator with additional permanent magnets: working principle, design and testing", Revue Roumaine des Sciences Techniques, Série Électrotechnique et Énergétique, Vol. 62, No. 1, 2017, pp 3 – 7.
[7] – D. Nicolescu, A. Radulian, M. Maricaru, S. Pricã, "High Force Heavy Duty Direct Current Actuator", Revue Roumaine des Sciences Techniques, Série Électrotechnique et Énergétique, Vol. 66, No. 1, 2021, pp. 139 – 143.
[8] – Z Wang, L. Sun, S. He, Y. Geng, Z. Liu, "A permanent Magnetic Actuator for 126 kV Vacuum Circuit Breakers", IEEE Transactions on Magnetics, Vol. 50, No. 3, 2014, pp 129-135.
[9] – D. Nicolescu, A. Radulian, C. Sărăcin, M. Maricaru, "New Solution of High Force Linear Actuator with Permanent Magnets", Revue Roumaine des Sciences Techniques, Série Électrotechnique et Énergétique, Vol. 69, No. 2, 2024, pp. 165 – 170.
[10] – G. Zeng, Y. Xiangyu, H. Yin, Y. Jing, S. Zhao, J. Cao, "Unsymmetrical bistable multimagnetic circuit permanent magnet actuator for high – voltage circuit breaker application: analysis, design, and dynamic simulation", IET Electric Power Applications, Vol. 14, No. 5, 2020, pp. 827 – 836.
[11] – G. Wang, E. Dong, Y. Wang, S. Yin, L. Zhang, T. Qin "A new Dynamic Displacement Prediction Method for Contactors with Constant Air Gap", International Journal of Applied Electromagnetics and Mechanics, Vol. 69, No. 4, 2022.
[12] – L.R. Neiman, P.L. Kalantarov, "Bazele Teoretice ale Electrotehnicii", Editura Energetică de Stat, Moscova, 1955.
[13] – G. Zeng, X. Yang, "Analysis, Design and Optimization of a Novel Asymmetrical Bistrable Short Mover Permanent Magnet Actuator for High – Voltage Circuit Breaker Application", MDPI – Actuators, Vol. 11, No. 7, 2022.
[14] – D. Meeker, "Finite Element Method Magnetics, Version 4.2 – User's Manual, 2018" [online], citat la 08.11.2022, disponibil la URL: https://www.femm.info/wiki/Documentation/
[15] – M. Rong, J. Lou, Y. Liu, J. Li, "Static and Dynamic Analysis for Contactor with a New Type of Permanent Magnet Actuator", IEICE Transactions on Electronics, Vol. E89-C, No. 8, pp 1210 – 1216.

[16] – C. Hou, J. Sun, Y. Cao, X. Liu, E. Wang, "Design and Analyses on Permanent Magnet Actuator for Mining Vacuum Circuit Breaker", 22nd International Symposium on Discharges and Electrical Insulation in Vacuum (ISDEIV), Matsue, 2006, pp. 512 – 515.
[17] – K. – N. Park, J. – W. Son, S. – C. Hahn, "Dynamic Characteristic Analysis of Permanent Magnetic Actuators coupled Electromagnetic – mechanical Finite Element Method", International Conference on Electrical Machines and Systems, Incheon, 2010, pp. 1706 – 1709.
[18] – Z. Cai, S. Ma, J. Wang, "An Approach of Improve Permanent Magnetic Actuator of Vacuum Circuit Breaker", 23rd International Symposium on Discharges and Electrical Insulation in Vacuum (ISDEIV), Bucharest, Romania, 2008.
[19] – Z. Huang, X. Duan, J. Zou, M. Chen, "A permanent magnetic actuator with scheduled stroke curve for vacuum circuit breakers", 24th International Symposium on Discharges and Electrical Insulation in Vacuum (ISDEIV), Braunschweig, Germany, 2010, pp. 162 – 165.
[20] – S. Fang, M. Xia, H. Lin, S.L. Ho, "Analysis and design of a high-speed permanent magnet characteristic actuator using eddy current effect for high-voltage vacuum circuit breaker", IET Electric Power Applications, Vol. 10, No. 4, 2016, pp. 268 – 275.
[21] – E. Dong, T. Qin, Y. Wang, X. Duan, J. Zou, "Experimental Research on Speed Control of Vacuum Breaker", IEEE Transactions on Power Delivery, Vol. 28, No. 4, 2013.
[22] - H.K. Jung, "Optimal design and dynamic characteristic analysis of a new type electric actuator for high voltage circuit breaker", International Conference on Electrical Machines and Systems, Wuhan, China, 2008.